A gradient in glucose metabolism regulates hair cell morphology along the tonotopic axis of the developing cochlea

James DB O'Sullivan [1#], Thomas S Blacker [2], Claire Scott[1], Weise Chang[3], Mohi Ahmed [1] and Zoe F Mann [1*].

[1] Centre for Craniofacial and Regenerative Biology, King's College London, SE1 9RT, United Kingdom.
[2]Department of Physics and Astronomy, University College London, WC1E 6BT United Kingdom.
[3] National Institute for Deafness and other Communication Disorders, National Institutes of Health, Bethesda, MD USA 20892-2320.

[#] Equal primary author contribution

* Corresponding author: zoe.mann@kcl.ac.uk
Zoë F Mann, Ph.D
Centre for Craniofacial and Regenerative Biology
Faculty of Dentistry, Oral & Craniofacial Sciences
Guy's Hospital
Great Maze Road
London SE1 1UK, U.K.

Graded glycolysis regulates hair cell morphology along the tonotopic axis of the developing cochlea.

James DB O'Sullivan [1#], Thomas S Blacker [2], Claire Scott [1], Weise Chang [3], Mohi Ahmed [1], Val Yianni [1] and Zoe F Mann [1*].

[1] Centre for Craniofacial and Regenerative Biology, King's College London
[2] Department of Physics and Astronomy, University College London
[3] National Institute for Deafness and other Communication Disorders, National Institutes of Health
Corresponding author: zoe.mann@kcl.ac.uk

Abstract

In vertebrates with elongated auditory organs, mechanosensory hair cells (HCs) are organised such that complex sounds are broken down into their component frequencies along the basal-to-apical long (tonotopic) axis. Acquisition of frequency-specific morphologies at the appropriate positions along the chick cochlea, the basilar papilla (BP), requires that nascent HCs determine their tonotopic positions during development. The complex signalling within the auditory organ between the developing HC and its local niche along the axis is currently poorly understood. Here we apply NAD(P)H fluorescence lifetime imaging (FLIM) to reveal metabolic gradients along the tonotopic axis of the developing BP. Re-shaping these gradients during development, by inhibiting different branch points of glucose catabolism, alters normal Bmp7 and Chordin like-1 signalling leading to flattening of tonotopic patterning and hair cell morphology along the axis. These findings indicate a causal link between morphogen signalling and metabolic reprogramming in specifying tonotopic morphologies in developing auditory HCs.

Introduction

Hearing relies on the life-long function of mechanosensory hair cells (HCs) and their associated glial-like supporting cells (SCs) within the cochlea. In both mammals and birds, different frequencies stimulate HCs located at different positions along the basal-to-apical long axis of the auditory epithelium to separate complex sounds into their spectral components. This phenomenon, known as tonotopy, underlies our ability to differentiate between the high pitch of a mosquito and the low rumbling of thunder. The specific factors regulating the development of tonotopy remain, largely, unclear. As high frequency HCs show increased vulnerability to insults, including aging [1], noise damage [2,3] and ototoxicity [4], awareness of the mechanisms underlying the formation of frequency-specific HC properties is crucial to understanding both congenital auditory defects and HC regeneration. Enhanced knowledge of the pathways that drive specification of HC phenotypes at different frequency positions could identify novel strategies to preserve and restore high frequency hearing loss.

Metabolism, encompassing the complex network of chemical reactions that sustain life (summarised in Figure 1), has emerged as a key regulator of cell fate and differentiation [5]. Bidirectional signalling between metabolic networks and the epigenome has been extensively studied in models of cancer cell biology and tumorigenesis [6]. A majority of chromatin modifying enzymes (involved in acetylation and methylation) that drive cell fate switches in cancer rely upon metabolic intermediates as co-factors or substrates, highlighting a link between cell metabolism and transcription [7]. Instructive roles for glucose metabolism and reprogramming between glycolytic and oxidative pathways have been reported in various systems during development, including delamination and migration in embryonic neural crest [8], hair cells in the zebrafish inner ear [9], specification of trophectoderm fate in the mouse embryo [10] and cell fate decisions associated with elongation of body axis and development of the tail bud [11-13]. However, the role of metabolism in cells of developing sensory epithelia in inner sense organs has not yet been fully explored. This is, in part, because the classic biochemical approaches from which our knowledge of metabolism has formed typically involve the destructive extraction of metabolites from a sample. Probing metabolism in this way, although valuable, means that the spatial organisation of metabolic pathways in complex tissues is lost. As the chick cochlea, the basilar papilla (BP), contains multiple cell types, investigating the regulation of cell fate by metabolism requires experimental approaches capable of interrogating metabolic pathways in live preparations with single cell resolution.

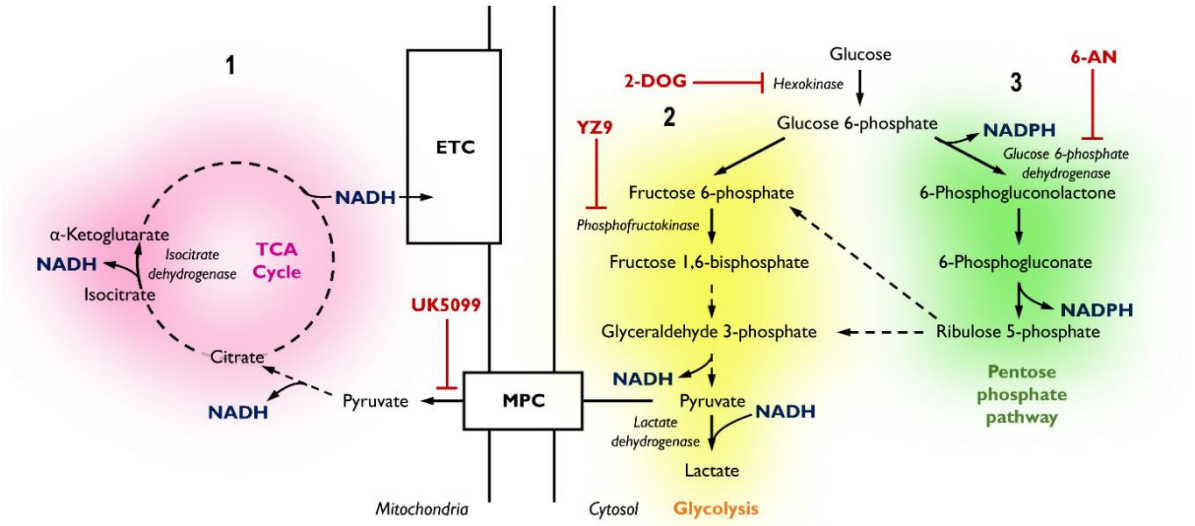

Figure 1. Main metabolic pathways that regulate cellular NADPH/NADH.
(pink) - Glucose metabolism in mitochondria. Following its conversion from glucose in glycolysis, pyruvate enters mitochondria via the mitochondrial pyruvate carrier (MPC) and enters the tricarboxylic acid (TCA) cycle. Its sequential oxidation provides reducing equivalents in the form of NADH to the electron transport chain (ETC), driving ATP production by oxidative phosphorylation (OXPHOS).
(yellow) - Cytosolic glycolysis. In this process, one molecule of glucose is anaerobically converted into two molecules of pyruvate to yield two molecules of ATP. Lactate dehydrogenase (LDH) acts to maintain the pool of NAD+ necessary for glycolysis to take place by oxidising NADH upon the reduction of pyruvate to lactate.
(green) - Glucose flux via the pentose phosphate pathway (PPP). Running parallel to glycolysis, the PPP branches from glycolysis via glucose 6-phosphate (G6P), generating NADPH and ribose 5-phosphate (R5P),

shunting carbons back to glycolysis at glyceraldehyde 3-phosphate and fructose 1,6-bisphosphate. The PPP is a major regulator for cellular redox homeostasis.
Metabolic pathways targeted for pharmacological intervention and their corresponding inhibitors are indicated for each pathway (UK5099, YZ9, 2-DOG, 6-AN).

We have previously demonstrated that fluorescence lifetime imaging microscopy (FLIM) can be utilised as a label-free means to identify metabolic alterations in the cell types of the inner ear by spatially resolving differences in the fluorescence decay of the reduced redox cofactors nicotinamide adenine dinucleotide (NADH) and its phosphorylated analogue NADPH (Figure 1) [14]. Here, we apply this technique to investigate a role for metabolism in specifying proximal (high frequency) verses distal (low frequency) HCs, using previously defined morphological markers of tonotopy as read-outs for HC phenotype [15,16] . We first use NAD(P)H FLIM to identify a gradient in NADPH-linked metabolism along the tonotopic axis of the developing chick cochlea. Consistent with previous research, the metabolic gradients we identified could not be explained by gradients of metabolic mRNAs and the expression patterns of metabolic effector proteins along the tonotopic axis. Neither were they correlated with mitochondrial activity, suggesting an origin in the cytosol. We therefore systematically interrogated the nature and roles of these gradients by modulating metabolic flux through different branches of glucose catabolism at key stages in HC formation. We found that the balance of glucose flux between the pentose phosphate pathway (PPP) and the main branch of glycolysis (Figure 1) instructs tonotopic HC morphologies by regulating the graded expression of Bmp7 and its antagonist Chordin-like-1, known determinants of tonotopic identity [17]. Our findings highlight a novel role for cytosolic glucose metabolism in specifying HC positional identity and provide the first characterisation of unique metabolic states associated with the emergence of HC and SC lineages.

Results

NAD(P)H FLIM reveals differences in the cellular balance between NADPH and NADH along the tonotopic axis of the developing BP.

NAD and NADP are metabolic cofactors responsible for ferrying reducing equivalents between intracellular redox reactions throughout the cellular metabolic network (Figure 1). The two molecules are fluorescent in their reduced (electron-carrying) forms NADH and NADPH, a feature that is lost upon oxidation to NAD+ and NADP+. The spectral properties of NADH and NADPH are identical, meaning that their combined signal emitted from living cells is labelled as NAD(P)H. FLIM of NAD(P)H has shown significant promise for identifying changes in the metabolic pathways active at a given instance in living cells. This technique measures the evolution of the NAD(P)H fluorescence signal over nanosecond time scales following excitation by a laser pulse. The average rate of photon decay is

known as the fluorescence lifetime, a property that is highly sensitive to the local environment of the emitting molecule.

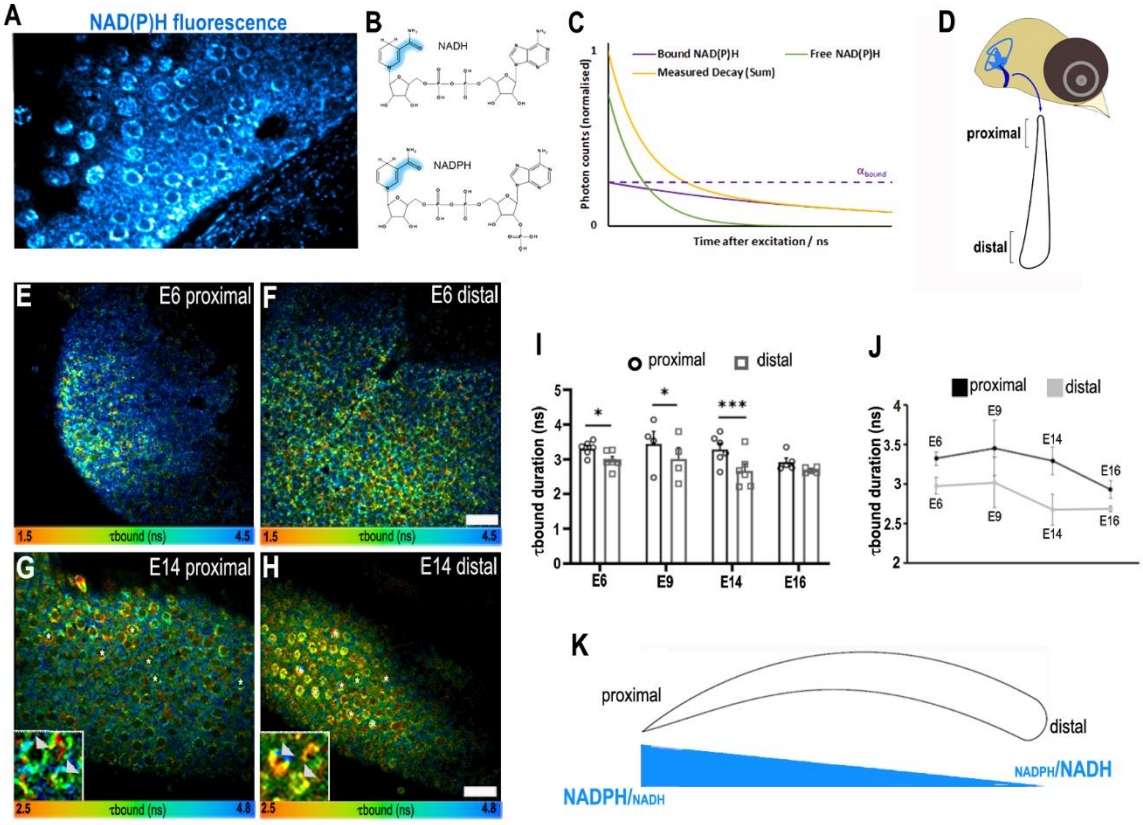

Figure 2. A proximal-to-distal metabolic gradient in the developing chick cochlea.
(A) Two-photon fluorescence image showing NAD(P)H in a live BP explant at E14.
(B) Inherent fluorescence from NADH and NADPH.
(C) NAD(P)H FLIM resolves two components corresponding to freely diffusing (shorter lifetime, τ_{free}) and enzyme bound (longer lifetime, τ_{bound}). The relative proportion of these components is labelled α_{bound}. Changes in τ_{bound} and α_{bound} imply changes in metabolic state.
(D) Schematic of the chick BP, indicating the proximal and distal regions.
(E-H) FLIM images of the bound NAD(P)H fluorescence lifetime signal τ_{bound} in the proximal and distal BP regions at E6 and E14. White asterisks indicate the HCs. Higher magnification images highlight the differences in τ_{bound} lifetime between proximal and distal HCs at E14.
(I-J) Quantification of τ_{bound} during development shows a shift from NADPH to NADH producing pathways. Line graphs highlight differences in τ_{bound} between proximal (black) and distal (grey) BP regions throughout development. Scale bars = 50µm. Data are mean ± SEM; E6: n = 6, E9: n= 4, E14: n = 7 and E16: n = 6 biological replicates. ***** $p < 0.05$ 2-way ANOVA. E16 $p = 0.05$ 2-way ANOVA.
(K) Schematic showing the tonotopic gradient in cellular NADPH/NADH along the tonotopic axis.

NAD(P)H FLIM typically resolves two fluorescence lifetime components in live cells and tissues (Figure 2A-D); one with a duration of around 0.4 ns from freely diffusing NAD(P)H (labelled τ_{free}) and the other of 2 ns or more from the pool of NAD(P)H that is bound to enzymes or cofactors (τ_{bound}) [18,19] (Figure 2C). Changes in the value of τ_{bound} and the relative proportion of bound species in a cell labelled α_{bound}, indicate switching in the enzyme families to which NADH and NADPH are bound. NAD(P)H FLIM therefore provide a readout for alterations in cellular metabolism in live cells as they carry out their

various functions. We used NAD(P)H FLIM to monitor metabolism in developing HCs and SCs along the proximal-to-distal (tonotopic) axis of the BP (Figure 2E-H). At E6, when cells in the BP begin acquiring their positional identity [17,20], we observed a significant ($p < 0.05$ 2-way repeated measures ANOVA) difference in τ_{bound} along the tonotopic axis (Figure 2D-I). The proximal-to-distal gradient in τ_{bound} (Figure 2D) was also evident at E9, when cells are post mitotic [21], and at E14, when HCs are considered fully differentiated (Figure 2G-J) ($p < 0.05$ 2-way ANOVA). The gradient observed in τ_{bound} throughout BP development, specifically at E6 and E9, is consistent with previous findings showing that graded morphogen signalling along the BP sets up HC positional identity between E6 and E8 [17,20]. As the fluorescence lifetime of enzyme bound NADPH inside the cell is significantly longer than that of bound NADH [22,23], changes in τ_{bound} report shifts in the cellular balance between NADPH/NADH [14]. These data therefore suggest a difference in NADPH-linked metabolism along the tonotopic axis of the developing BP.

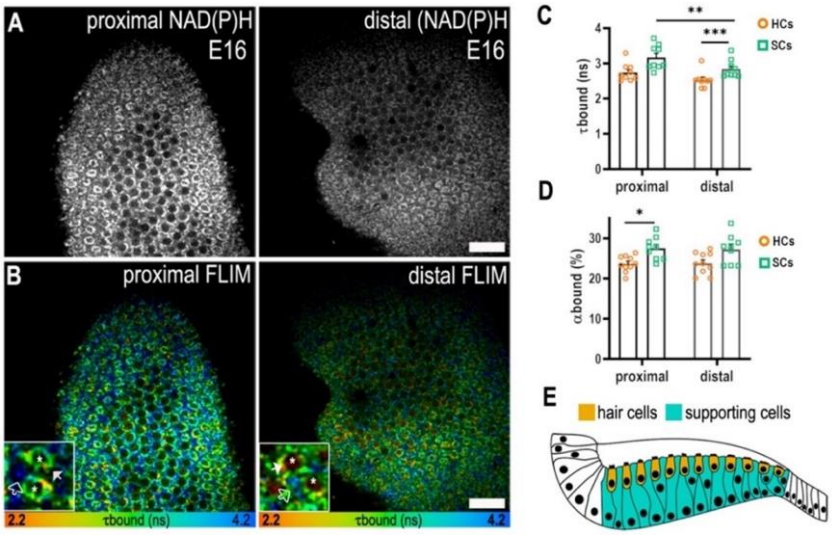

Figure 2 supplement 1. Metabolic differences between hair cells and supporting cells along the tonotopic axis of the developing chick cochlea.
(A) NAD(P)H fluorescence in the proximal and distal regions at E16.
(B) Mean FLIM signal for NAD(P)H in the proximal and distal BP. Images show the τ_{bound} and signal and are mapped using a pseudo colour time scale representing 2.2 and 4.2 ns. White boxes Highlight differences in mean lifetime between HCs (white asterisk, block arrows) and SCs (empty arrows).
(C) At E16, τ_{bound} is significantly higher in supporting cells (blue) compared to hair cells (orange), indicating distinct metabolic profiles between cell types.
(D) The cellular proportion of bound NAD(P)H (α_{bound}) is significantly higher in supporting (blue) compared to hair cells (orange).
(E) Schematic showing a cross-sectional view of the BP at E16. HCs (orange) and SCs (blue) are indicated. Pseudo colour scale reflects the lifetime duration. Warm colours indicate short lifetimes and cool colours longer lifetimes. Data are mean ± SEM. * $p < 0.05$, 2-way ANOVA, n = 10 biological replicates representative of 25 HCs and 25 SCs analysed from each independent biological replicate. Scale bars are 50μm.

As HCs and SCs are not easily identified within the epithelium at stages before E9 using FLIM (Figure 2 Supplement 1 E, F), cell-specific analysis was done at E16, when HCs and SCs can be distinguished (Figure 2 Supplement 1 A, B). At E16, we found that τ_{bound} (NADPH/NADH) differed significantly ($p <0.05$ 2-way repeated measures ANOVA) in the distal BP region and α_{bound} in the proximal BP region (Figure 2 Supplement 1C, D, E) indicating subtle differences in HC-SC metabolic coupling along the tonotopic axis. Additionally, at E16 we observed a tonotopic gradient ($p <0.05$ 2-way repeats measures ANOVA)

in τ_{bound} within SCs but not HCs (Figure 2 Supplement 1C). The PPP is a major source of cellular antioxidant defence. Given what we understand about the role of SCs in sensing and responding to HC stress [24], the increased NADPH]/[NADH] ratio in proximal SCs may reflect the greater need for antioxidant defence in high frequency HCs.

Live imaging of mitochondrial and cytosolic glucose metabolism along the tonotopic axis of the developing BP.

Cellular NADPH/NADH is highly interrelated with cytosolic glycolysis and mitochondrial oxidative phosphorylation (OXPHOS)[25] (Figure 1). To further characterise metabolism along the tonotopic axis and investigate potential crosstalk between mitochondrial OXPHOS, glycolysis and NADPH/NADH, we carried out live imaging in BP explants using the potentiometric fluorescent dye tetramethyl-rhodamine-methyl-ester (TMRM) and the fluorescent D-glucose derivative 2-[N-(7-nitrobenz-2-oxa-1,3-diazol-4-yl)-amino]-2-deoxy-D-glucose (2-NBDG)[26].

TMRM is a cell permeable dye that reports mitochondrial membrane potential ($\Delta\Psi_{mt}$), giving a direct read-out of glycolytically-derived pyruvate oxidation in the mitochondrial tricarboxylic acid (TCA) cycle and the activity of the mitochondrial electron transport chain (ETC) (Figure 1). 2-NBDG has been used extensively used to measure glucose transport across the plasma membrane in multiple cell types [26]. 2-NBDG enters cells via GLUT transporters in the plasma membrane, after which it is phosphorylated by Hexokinase (HK) the first rate-limiting step in cytosolic glycolysis (Figure 1). The fluorescent signal from 2-NBDG therefore reflects the rate of cellular glucose uptake, which can be correlated with its consumption [26]. For instance, tumour cells with elevated glucose metabolism via the Warburg effect exhibit elevated 2-NBDG uptake [26].

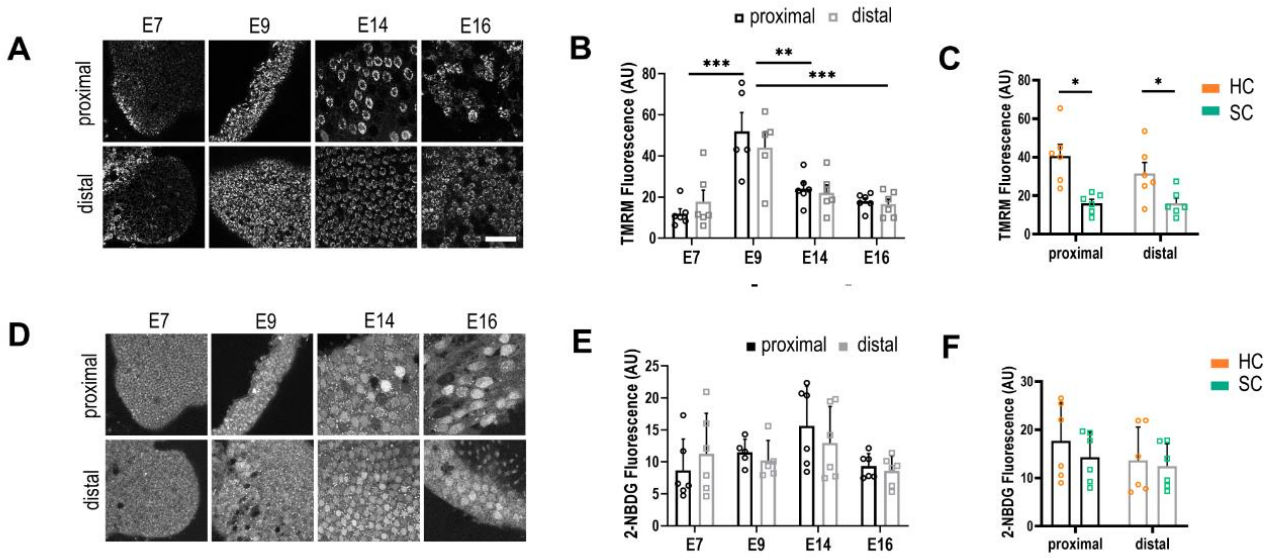

Figure 3. Live imaging of glucose metabolism in HCs and SCs at different positions along the tonotopic axis.
(A) Mitochondrial membrane potential (measured in the same cultures as in panel A) using TMRM fluorescence in single z-planes from image stacks in the proximal and distal regions of live BP explants.
(B) TMRM fluorescence indicates a significant increase in mitochondrial activity between E7 and E9, followed by significant decrease between E9 and E14.
(C) Differences in mitochondrial activity between HCs and SCs along the tonotopic axis.
(D) 2-NBDG labelling in live BP explants shows no difference in glucose uptake along the proximal-to-distal axis or between cell types during development.
(E) Quantification of glucose uptake during development.
(F) 2-NBDG fluorescence in hair cells (orange bars) and supporting cells (green bars) at E14.
Data are mean ± SEM. For TMRM n = 6 biological replicates for E7, E10, E14. * p = < 0.05 2-way ANOVA. HCs vs SCs, proximal: n = 6 biological replicates, * = p < 0.05 for proximal and distal regions 2-way ANOVA. E7 n=3, E10 n=3, E14 n=5, E16 n=5 biological replicates. * = p < 0.05 2-way ANOVA. Scale bars = 40 μm.

We dual-loaded BP explants with TMRM and 2-NBDG and analysed the combined fluorescence signal from single cells between E7 and E16 (Figure 3). TMRM fluorescence revealed no significant difference in $\Delta\Psi_{mt}$ between proximal and distal regions at any developmental stage (Figure 3 A-B). These findings indicate a uniform mitochondrial activity along the tonotopic axis throughout development suggesting that the gradient in NADPH/NADH reported by τ_{bound} (Figure 2 D-I) originates from differences in cytosolic and not mitochondrial glucose metabolism. Despite no difference between frequency regions, $\Delta\Psi_{mt}$ did change within the epithelium as a function of developmental age (Figure 3A-C). TMRM fluorescence reports increased activity in the mitochondrial ETC, which consumes more NADH. Changes in cellular NADH driven by enhanced OXPHOS in mitochondria have been proposed to reflect a shift in α_{bound} [18]. While the biochemical relationships linking α_{bound} to specific metabolic phenotypes and pathways are less established than those for τ_{bound}, correlations have been observed[18,27] in relation to the balance between glycolytic and oxidative ATP production. We therefore investigated whether the increased TMRM fluorescence correlated with a developmental shift in α_{bound}, where a higher α_{bound} indicates a more oxidative phenotype [18]. Our data revealed an increase in α_{bound} in cells of the

proximal and distal BP regions from E9 onwards, indicating a developmental switch towards more oxidative pathways (Figure 3 Supplement 1).

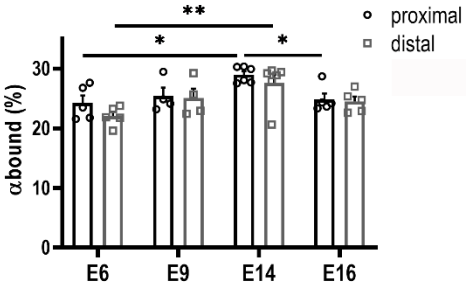

Figure 3 Supplement 1. Developmental changes in α_{bound} along the tonotopic axis of the chick BP.
α_{bound} increases significantly in both proximal (black) and distal (grey) BP regions between E6 and E14 and decreases significantly between E14 and E16. Data are mean ± SEM; E6: n = 6, E9: n= 4, E14: n = 7 and E16: n = 6 biological replicates. * $p < 0.05$ 2-way ANOVA. E16 p = 0.05 2-way ANOVA.

Analysis of TMRM fluorescence in HCs and SCs specifically revealed a consistently higher $\Delta\Psi_{mt}$ in fully differentiated HCs compared to SCs from E14 onwards (Figure 3C). To rule out whether of the intensity of TMRM fluorescence occurred due to differences in dye uptake via the HC transduction channel, explants were dual loaded with the permeant channel blocker FM1-43 [28] (Figure 3 Supplement 2).

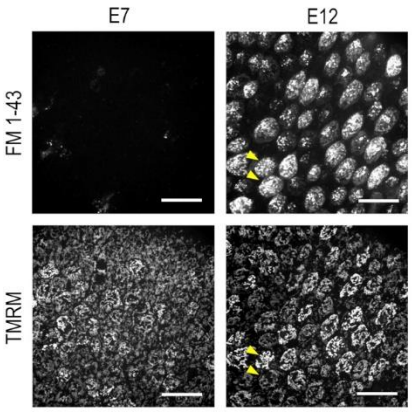

Figure 3 Supplement 2. TMRM fluorescence intensity is not dependent on uptake via the HC transduction channel.
Live BP explants at E7 and E12 dual loaded with the permeant MET channel blocker FM1-43 (top) and the mitochondrial membrane potential dye TMRM (bottom). Scale bars are 20μm.

Measuring the 2-NDBG fluorescence in the same cells revealed no differences in glucose uptake along the tonotopic axis at any developmental stage or between cell types (Figure 3D-F). This result, in combination with the gradient in NAD(P)H τ_{bound} identified using FLIM, indicates that the relative glucose flux between the PPP and the main glycolytic pathway must vary along the tonotopic axis.

Expression of metabolic effector proteins in the developing BP.

Metabolic reprogramming and the modulation of metabolic pathway activity is driven through post-translational modifications and changes in the cell-specific expression of metabolic effector proteins [29]. We therefore looked to validate our 2-NBDG and TMRM results at the protein level, and investigated developmental changes in the expression of lactate dehydrogenase isozymes alpha and beta (LDHA, LDHB) and isocitrate dehydrogenase 3 subunit A (IDH3A), known regulators of reprogramming between glycolysis and OXPHOS (Figure 4 A, Figure 4 Supplement 1)) [29]. We hypothesised that, given their regulatory roles in the switch between glycolytic and oxidative

metabolism [29-32], LDH and IDH3A expression levels would reflect whether the gradient we observed in FLIM could be accounted for by a switch between glycolysis and OXPHOS.

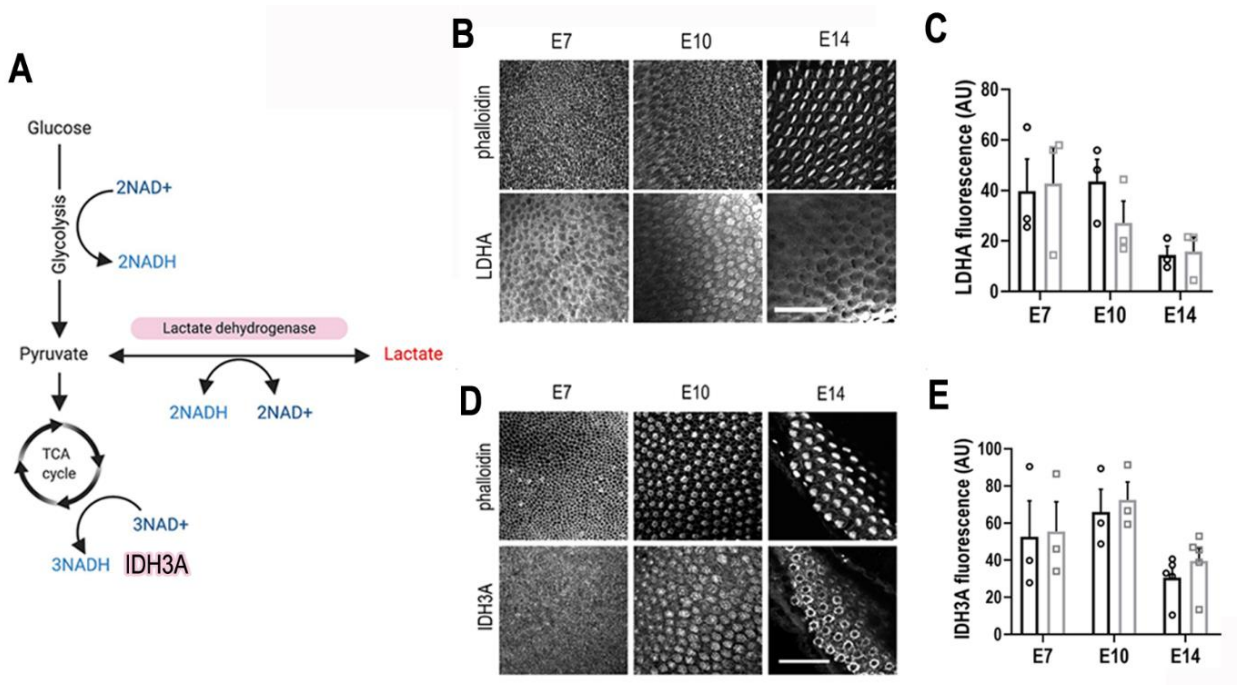

Figure 4. Developmental changes in expression of metabolic effector proteins.
(A) Functions of lactate dehydrogenase alpha (LDHA) and isocitrate dehydrogenase subunit A3 in cytosolic glucose metabolism.
(B) BP explants stained with Phalloidin and labelled for the metabolic enzyme LDHA. Phalloidin marks the HCs at different stages of cochlear development (E7-E14). At E7, LDHA expression is localised to SCs. By E10 expression appears restricted to the HCs.
(C) No differences in LDHA expression were evident along the proximal-to-distal axis of the BP at early developmental stages. Reflecting a reprogramming of glycolysis, LDHA expression reduced significantly in the proximal (black bars) but not distal (grey bars) region at E14. Data are mean ± SEM. * $p < 0.05$ 2-way ANOVA. Scale bar is 50 µm
(D) BP explants stained with Phalloidin and labelled for IDH3A in proximal and distal BP regions between E7-E14.
(G) Quantification of IDH3A expression in proximal (black bars) and distal (grey bars) BP regions throughout development. E14 n=5. E16 n=3 independent biological replicates. $p < 0.05$ 2-way ANOVA. Scale bars = 40 µm.

During development, LDHA activity is upregulated to maintain NAD^+ levels and increase glycolysis when cells cannot rely on OXPHOS [33]. We observed no significant difference in LDHA protein expression between proximal and distal regions at any developmental stage (Figure 4 B, C).

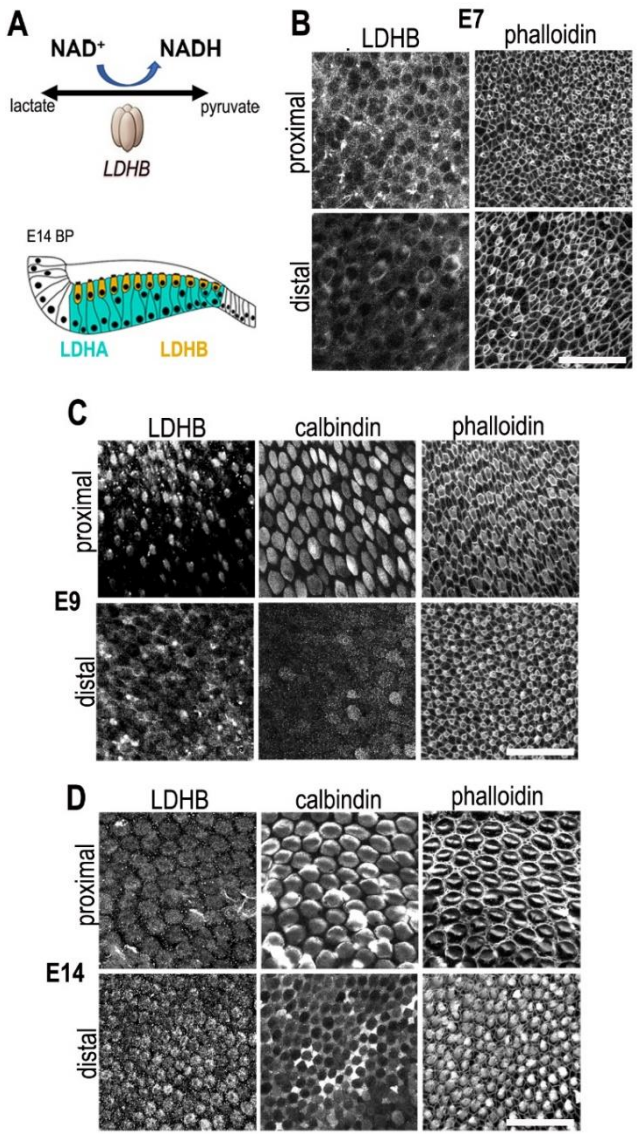

Figure 4 supplement 1. Developmental changes in expression pattern of LDHB.
(A) The role of lactate dehydrogenase beta (LDHB) in converting lactate to pyruvate. Schematic shows the pattern of LDHA (blue) and LDHB (orange) expression in HCs and SCs at E14.
(B) BP whole-mounts stained with Phalloidin and labelled for the metabolic enzyme LDHB in the proximal and distal BP regions at E7.
(C-D) BP whole-mounts labelled with Phalloidin and stained for LDHB and the calcium binding protein Calbindin in proximal and distal regions at E9 and E14.

Instead, the cell-specific expression of LDHA changed from SCs to HCs between E7 and E10 becoming restricted to SCs again between E10 and E14 (Figure 4 B, C). Compared to LDHA, the expression of LDHB was restricted to HCs at E9 and E14, a phenotype associated with enhanced OXPHOS. The mechanisms regulating these changes are not known, but their timing correlates highly with key stages in HC development [34]. In certain cancer models [35] and in cells of the developing embryo [36], downregulation of IDH3A is linked with a switch from oxidative to glycolytic metabolism. This occurs due to a reduced glucose flux in the mitochondrial TCA cycle [32]. We observed no significant differences in IDH3A protein expression between proximal and distal regions during development (Figure 5E) and did not detect expression of IDH3B mRNA or protein in the sensory epithelium at any stage before E14 (data not shown).

The restriction of LDHB and IDH3a to HCs throughout development (Figure 4, Figure 4 Supplement 1) further supports the increased OXPHOS in this cell type. Overall, our analysis of protein expression suggests that the proximal-distal gradient in NADPH is not driven by a switch between glycolytic and oxidative metabolism along the BP. However, the differences in metabolic state observed between HCs and SCs from E14 onwards are consistent with increased reliance of HCs on OXPHOS as they become functionally mature.

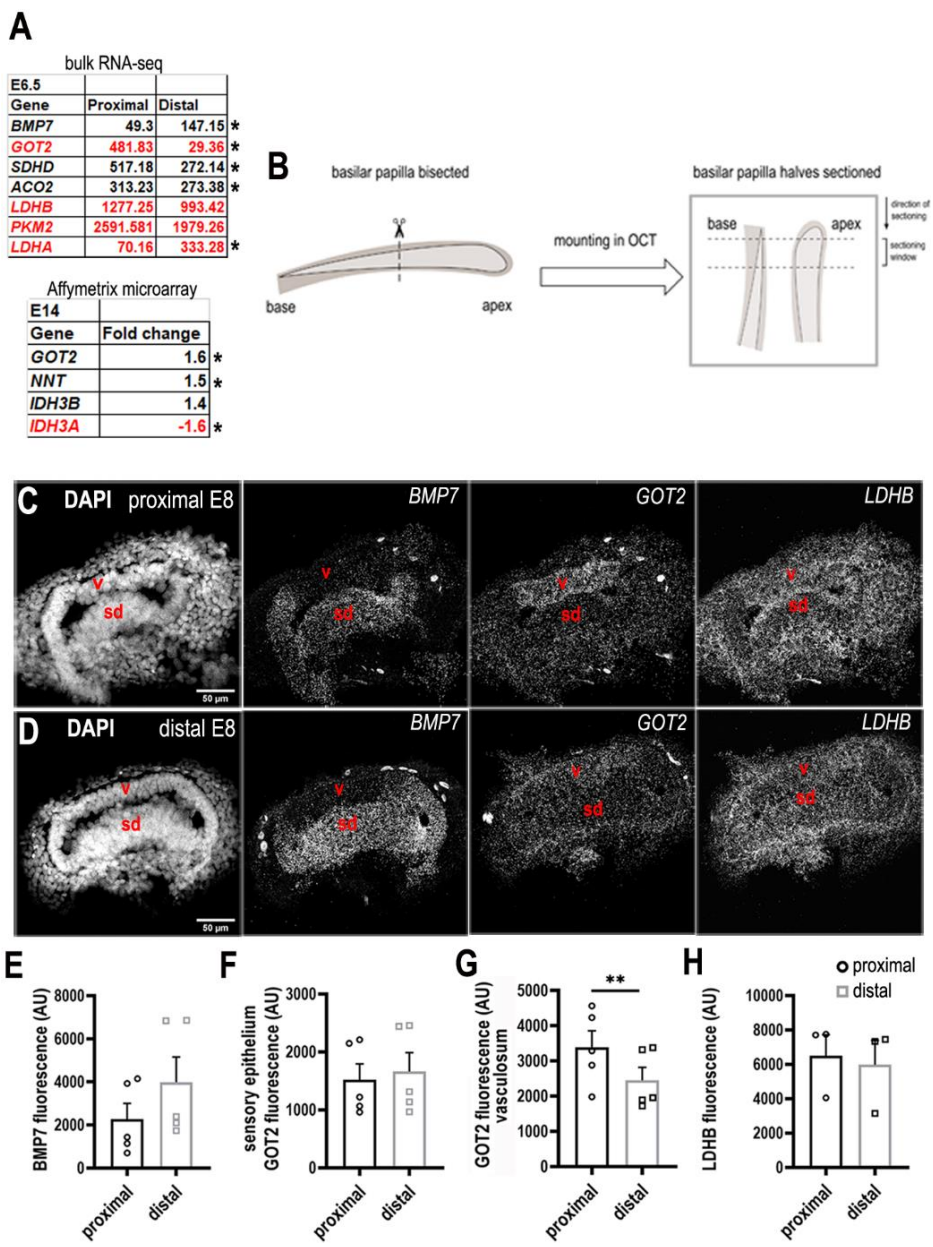

Figure 5. Differential expression of metabolic mRNAs along the tonotopic axis of the chick basilar papilla. **(A Top)** Metabolic genes with differential expression between proximal and distal BP regions. Data show normalised RPKM values in the proximal and distal BP regions at E6.
(A bottom) Affymetrix microarray data showing the fold change in expression of each transcript at the proximal compared to the distal region of the BP at E14.
(B) Sectioning protocol used to collect samples from proximal and distal regions at E8. Proximal and distal tissue used for RNA scope was collected and processed simultaneously from within the same BP.
(C-D) RNA scope analysis of metabolic regulatory proteins in the developing BP. Images show metabolic mRNA expression in comparative cross sections from proximal and distal BP regions at E8. * = $p < 0.05$. 2-way ANOVA
(E-H) Quantification of RNA scope fluorescence in the sensory epithelium at proximal and distal regions. The sensory epithelium (se) and vasculosa (v) were identified morphologically using the DAPI channel.
BMP7 – Bone morphogenetic protein 7, GOT2 - Glutamic-Oxaloacetic Transaminase 2, SDHD – Succinate dehydrogenase complex subunit D, ACO2 – Aconitase 2 LDHB – Lactate dehydrogenase beta, PKM2 – Pyruvate kinase M2, LDHA – Lactate dehydrogenase alpha, NNT - Nicotinamide Nucleotide Transhydrogenase, IDH3B – Isocitrate dehydrogenase beta, IDH3A - Isocitrate dehydrogenase alpha. Transcripts annotated red indicates those involved in regulating cellular NADPH/NADH.

Tonotopic expression of metabolic mRNAs along the proximal-to-distal axis of the developing BP.

NAD(P)H FLIM (Figure 2) and the immunofluorescence measurements above (Figure 4, Figure 4 supplement 1) identified tonotopic and cell-specific differences in glucose metabolism which could not be attributed to switching between glycolysis and OXPHOS. To further probe the biochemical basis for this gradient, and investigate metabolic differences along the tonotopic axis, we exploited existing transcriptional data sets for proximal and distal regions of the developing BP [17]. Data were analysed for differential expression of metabolic mRNAs involved in NADPH regulation at E6.5 and E14 (Figure 5 A). Prior to mRNA isolation for bulk RNA-seq and Affymetrix microarray analysis, BPs were separated into proximal, middle, and distal thirds [17]. Microarray data were analysed to identify transcripts with expression levels at least two-fold higher in the proximal compared to distal half of the BP. From the combined data sets, we identified multiple genes with differential expression between proximal and distal regions involved in regulating cellular NADPH and cellular redox (Figure 5A).

Overall, metabolic genes showing the highest differential expression between proximal and distal regions were those involved in cytosolic glycolysis and redox homeostasis (Figure 4A) and would be consistent with the higher τ_{bound} reported for the proximal BP region (Figure 2I). However, as these expression data were obtained from bulk RNA-seq analysis, they do not provide the necessary spatial resolution to determine mRNA expression in different cochlear cell types and regions. To visualise the cell and region-specific expression of metabolic mRNAs involved in cytosolic glycolysis (LDHB) and redox homeostasis (GOT2, PKM2, NNT), we performed RNA scope analysis in cross-sections from proximal and distal BP regions (Figure 5B-D). RNA scope for BMP7 was used as an internal control, as we know this transcript is expressed in a distal-to-proximal gradient along the sensory epithelium [17]. Although the expression of GOT2, LDHB and PKM2 (data not shown) exhibited trends consistent with their proposed relation to the FLIM signal along the tonotopic axis (Figure 5C-H), no significant differences were observed between regions. Additionally, a gene involved in OXPHOS, GOT2 (Figure 5F, G), showed strong expression only in structures outside the sensory epithelium including the vasculosa and the nerve fibres. It is unlikely therefore that these genes regulate metabolism in cells of the developing sensory epithelium. Therefore, both bulk and spatial analyses of metabolic mRNAs revealed no clear transcriptional basis for the proximal-to-distal FLIM gradient in τ_{bound} within the developing sensory epithelium.

Cytosolic glucose metabolism is necessary for tonotopic patterning in the chick cochlea.

Since we could not detect an obvious transcriptional basis for the proximal-distal gradient in NADPH, we sought to further characterise metabolism in the developing BP by investigating a functional role

in tonotopic patterning using systematic inhibition of different metabolic pathways. First, we blocked cytosolic glucose metabolism in BP explants using 2-deoxy-d-glucose (2-DOG), an inhibitor of hexokinase (HK)[37]. Explants were established at E6.5 and maintained for 7 days *in vitro* to the equivalent of E13.5 in control medium or that containing 2mM 2-DOG with 5mM sodium pyruvate (NaP), which ensures adequate substrate supply to the TCA cycle. In a normal BP, proximal HCs have larger surface areas and are more sparsely populated compared to those the distal region [15,16]. These morphological gradients are recapitulated in BP explant cultures during development [17]. Here, these metrics were determined by measuring differences in the HC luminal surface area, the size of HC nuclei and the HC density within defined ROIs (100 x100 μm^2) along the length of the organ. Luminal surface area was measured using phalloidin staining at the cuticular plate and nuclear size with DAPI (Figure 6 B-D). In control cultures, HCs developed with the normal tonotopic morphologies (luminal surface area, nuclear size and gross bundle morphology) (Figure 6A, C, D, Figure 6 Supplement 1).

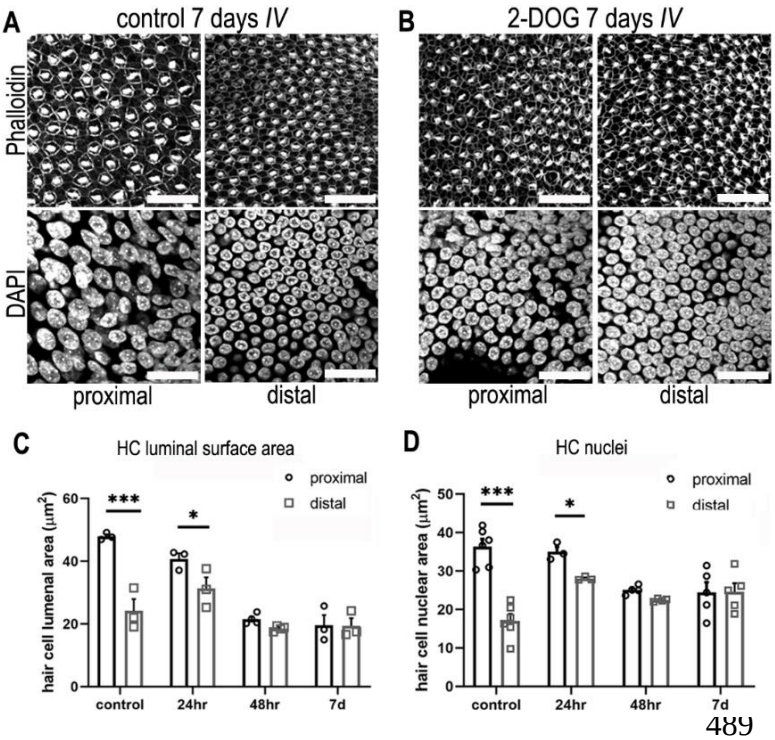

Figure 6. Blocking glycolysis at key stages of cochlear development induces distal-like phenotypes in the proximal BP.

(A-B) Maximum z-projections of BP explants showing Phalloidin and DAPI staining in the proximal and distal regions. Explants were maintained from E6.5 for 7 days *in vitro* (equivalent to E13.5) in either control medium or medium supplemented with 2mM 2-DOG + 5 mM Sodium Pyruvate (NaP). Phalloidin staining depicts differences in hair cell morphology between proximal and distal regions and DAPI indicates the gradient in hair cell size.

(C) Quantification of these differences**.** Hair cell luminal surface area was measured in 2500 μm^2 areas in the proximal (black bars) and distal (grey bars) BP regions for all culture conditions. In controls, mean hair cell luminal surface decreases progressively from the proximal-to-distal region. This gradient is abolished if glycolysis is blocked with 2-DOG between E6.5 and E13.5. 2-DOG caused a significant decrease in hair cell size in the proximal but not distal region. 2-DOG treatments were reduced to 24 or 48 hours to identify the developmental time window during which glycolysis takes effect. Following wash-out of 2-DOG after 24h, explants developed with normal hair cell positional identity and showed a significant decrease in luminal surface area along the proximal-to-distal axis. Explants treated with 2-DOG for 48 hours showed no recovery of positional identity following wash-out indicated by the loss of gradient in hair cell morphology.

(D) Quantification of HC nuclei area in the same 2500 μm^2 ROI. Treatment with 2DOG induced similar, yet less pronounced effects to those seen at the HC cuticular plate.

Data are mean ± SEM. ***** $p < 0.05$ 2-way ANOVA. Controls; n = 4, 2-DOG; n = 5, 24 2-DOG, n = 3 and 48h 2-DOG; n = 3 biological replicates. To ensure adequate substrate supply to the TCA cycle, 2-DOG-treated explants were supplemented with NaP. G6P glucose 6-phosphate, F6P – fructose 6-phosphate, F16BP – fructose 1,6-bisphosphate, 2-DOG – 2-deoxyglucose. Scale bars are 20 μm.

In contrast, when glycolysis was blocked between E6.5 and E13.5 equivalent, tonotopic patterning was abolished. This was indicated by the apparent flattening of HC phenotypes and a uniformly more distal-like morphology along the BP. In addition to changes in HC morphology, treatment with 2-DOG caused a significant ($p < 0.05$ 2-way ANOVA) increase in HC density in the proximal but not distal BP region (Figure 6 Supplement 2) again consistent with loss of tonotopic patterning along the organ.

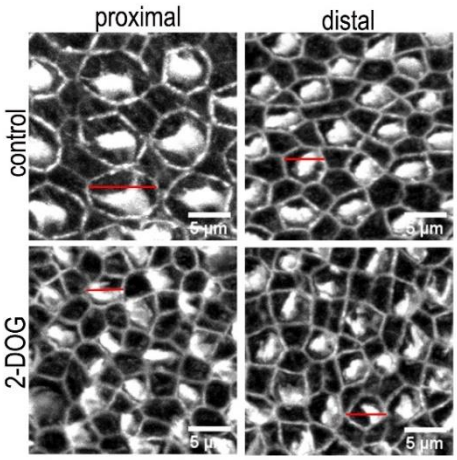

Figure 6 Supplement 1. Morphological differences in the HC bundle and cuticular plate region in BP explants treated with control or 2-DOG containing medium. Images are Maximum z-projections of Phalloidin stained BP explants from the proximal and distal BP regions. Explants were maintained from E6.5 for 7 days *in vitro* (equivalent to E13.5) in either control medium or that supplemented with 2mM 2-DOG + 5 mM Sodium Pyruvate (NaP). Phalloidin staining depicts differences in hair cell luminal surface area and gross bundle morphology between proximal and distal regions. Red lines indicate the size difference in HC luminal surface area between control and 2-DOG-treared cultures.

As changes in glucose metabolism have been linked with reduced cellular proliferation [38] we investigated the effects of 2-DOG on proliferation in developing BP explants. We hypothesised that because the majority of cells in the BP are postmitotic by E10 [21], adding EdU to cultures in the presence and absence of 2-DOG for 48h hours between E8 and E10 would capture any differences in proliferative capacity. We observed a consistent reduction in proliferation throughout the whole explant when glycolysis was blocked with 2-DOG (Figure 6 supplement 2). Increased proliferation therefore is unlikely to account for the higher cell density observed in the proximal region following inhibition of glycolysis. Further studies are needed to determine the specific mechanisms underlying this frequency-specific increase in HC density.

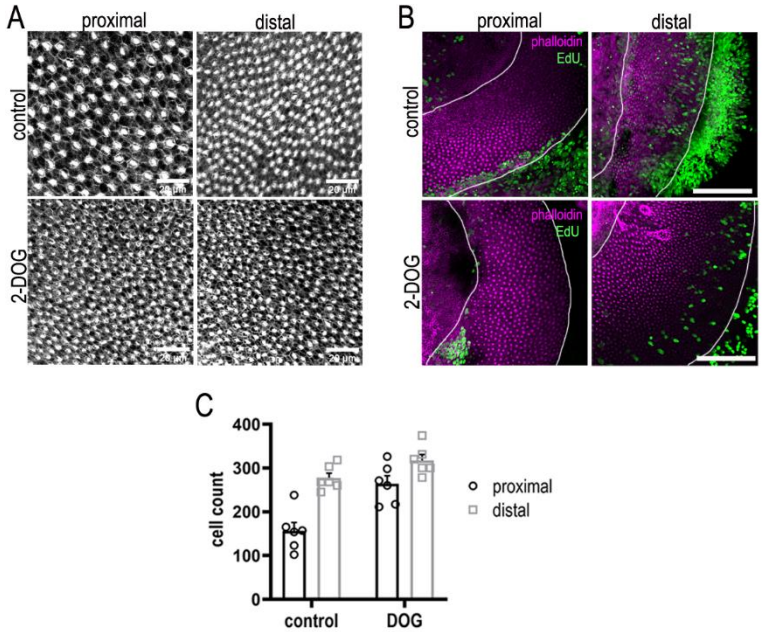

Figure 6 supplement 2. 2-DOG increases HC cell density in the proximal BP region independently of proliferation.
(A) Phalloidin staining indicating HC density in the proximal and distal BP regions in control (top) and 2-DOG treated (bottom) explants.
(B) Maximum z-projections of proximal and distal regions from Phalloidin (magenta) and the EdU (green) stained BPs. Explant cultures were established at E8 and maintained for 48 hours *in vitro* in control medium +EdU or medium containing EdU + 2mM 2-DOG and 5 mM sodium pyruvate. Proliferation was consistently reduced in 2-DOG treated explants. **(C)** (B) Quantification of HC density in proximal and distal BP regions counted from 100, 000 μm^2 ROIs in each region. Data mean ± sem. * = $p < 0.05$ 2-way ANOVA. Control: n = 6 biological replicates, 2-DOG: n = 6 biological replicates. EdU: control n= 4 independent biological replicates; 2DOG n = 4 independent biological replicates. White lines outline the regions of BP sensory epithelium.

Reciprocal morphogen gradients of Bmp7 and Chordin like-1 (Chdl-1) are known to establish tonotopy in the BP between E6.5 and E8 [17]. To determine whether cytosolic glucose metabolism acts during this same developmental window, we blocked HK activity for defined periods during BP development. Explants were established at E6.5 and treated with 2-DOG + sodium pyruvate for either 24 or 48 hours followed by wash out with control medium. These treatments correspond to the developmental window (E6.5-E8) described previously for refinement of tonotopic morphologies along the proximal-to-distal axis [17]. The gradient in HC morphology developed normally in BPs treated with 2-DOG for 24 hours but was absent in those treated for 48 hours (Figure 6 C-D). These results suggest that glucose metabolism acts within the same developmental time window as Bmp7 and Chdl-1, to set up tonotopic patterning along the BP. These findings are also consistent metabolically with the proximal-to-distal gradient in NADPH/NADH (τ_{bound}) observed at E6 and E9 (Figure 2I).

To further confirm a role for glucose catabolism in establishing HC positional identity, we employed a second method of modulating its activity that is independent of HK [39]. Glycolysis can also be blocked indirectly by raising cytosolic levels of the metabolite s-adenosyl methionine (SAM). Consistent with 2-DOG treatment, explants incubated with SAM between E6.5 and E13.5 lacked correct tonotopic patterning indicated by the flattening of HC morphologies along the tonotopic axis (Figure 6 supplement 3).

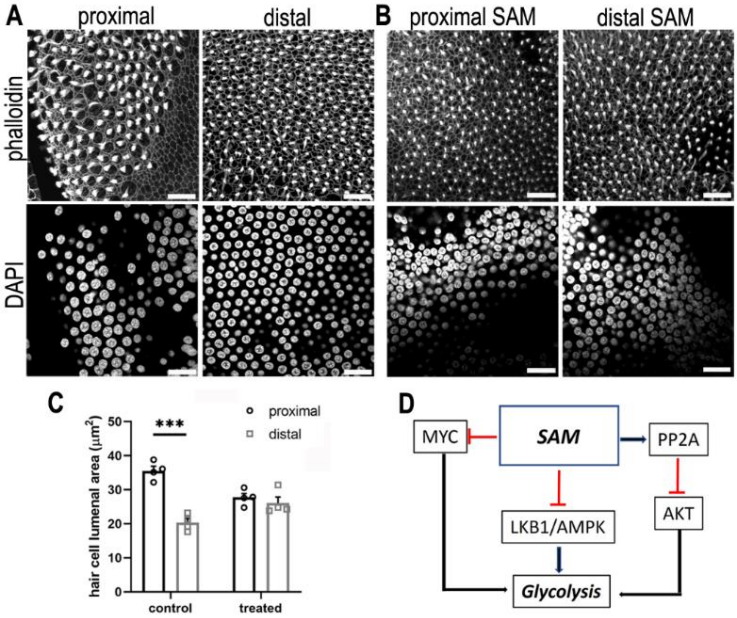

Figure 6 Supplement 3. Modulating S-Adenosyl methionine during development abolishes the gradient in hair cell morphology along the tonotopic axis of the BP.

(A-B) Images are maximal z-projections of proximal and distal regions from BP explants maintained for 7 days *in vitro* in control medium or medium containing 50 µM SAM. Phalloidin staining (A, B top panels) shows the BP surface and hair cell luminal surface areas and DAPI staining (A, B bottom panels) shows the hair cell size and density along the proximal-to-distal axis.

(C) Treatment of explants with SAM from E6.5 for 7 days *in vitro* abolished the normal gradient in hair luminal surface area along the tonotopic axis. This effect was most pronounced in the proximal compared to distal region. Hair cell luminal surface areas were measured from 2500 µm^2 areas in the proximal (black bars) and distal (grey bars) BP regions of control and SAM-treated explants.

(D) Schematic showing how increasing SAM levels indirectly modulates glycolytic flux.

Data are mean ± SEM. ***** $p < 0.05$ 2-way ANOVA. Controls: n = 5 and SAM: n = 4 biological replicates. Scale bars are 20 µm. MYC - MYC Proto-Oncogene, BHLH Transcription Factor, SAM - S-Adenosyl methionine, PP2A – protein phosphatase 2, AKT - *Akt* serine/threonine kinase family, LKB1/AMPK – serine threonine kinase pathway in volved in metabolic regulation.

Flux through the PPP is important for tonotopic patterning along the BP

Glucose metabolism encompasses glycolysis and the PPP in the cytosol and the TCA cycle in mitochondria, all of which are affected by treatment with 2-DOG. Recent studies in other systems have linked both the PPP and TCA cycle with cell fate decisions during development and differentiation [10,40]. We therefore sought to further dissect the metabolic signalling network during specification of tonotopy in the developing BP. To investigate a role for PPP-linked glucose metabolism, BP explants were established as described, and treated with 50 mM 6 Aminonicotinamide (6-AN) between E6.5 and E13.5 equivalent. Treatment with 6-AN inhibits the rate-limiting PPP enzyme glucose-6-phosphate dehydrogenase (G6PD) (Figure 1 panel 3). By comparison with control cultures, inhibition of PPP metabolism caused a significant decrease in hair cell size within 2500 µm^2 areas measured in the proximal BP (Figure 7 & Figure 7 Supplement 1). To determine whether this effect was specific to glucose flux through the PPP we also blocked phosphofrucktokinase (PFK), a rate limiting enzyme further down in the glycolytic pathway, using 1mM YZ9 (Figure 7 Supplement 2). Blocking PFK activity inhibits the glycolytic cascade involved in pyruvate production but does not change the activity of G6PD in the PPP [10]. YZ9 treatment resulted in a reduction in HC size, especially in the proximal region leading to a reduction in the HC gradient when analysed using pairwise comparisons (Sidak's multiple comparisons, p=0.17, Supplementary Table 1).

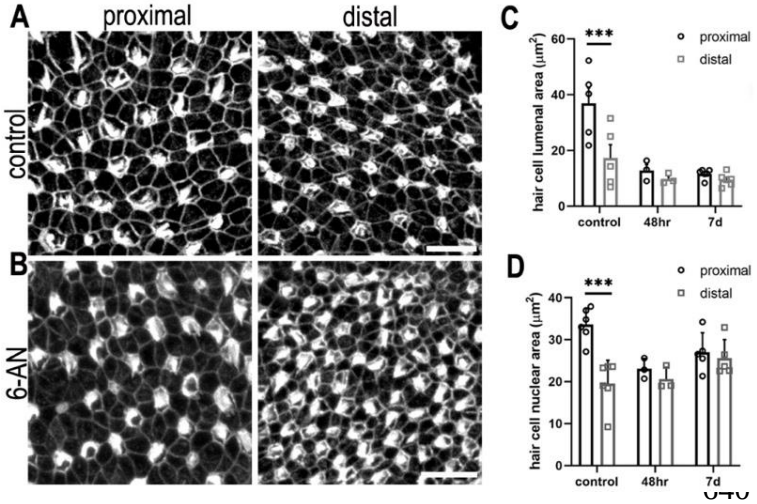

Figure 7. Glycolytic flux through the pentose phosphate pathway modulates hair cell development and positional identity along the tonotopic axis of the BP.
(A-B) Maximal z-projections of BP explants cultured from E6.5 for 7 days *in vitro* with control medium or medium containing 2 μM 6-AN. Images show the epithelial surface in proximal and distal BP regions stained with Phalloidin.
(C) Treatment of explants with 6-AN, a specific blocker of glycolytic flux through the pentose phosphate pathway, caused a significant reduction in proximal compared to distal hair cell luminal surface area. **(D)** Quantification of hair cell size using measurement of the cuticular plate in defined 2500^2 μm areas in the proximal (black bars) and distal (grey bars) BP regions. Hair cell luminal surface area was quantified using Phalloidin staining. Data are mean ± SEM. * $p < 0.05$ 2-way ANOVA. Controls: n = 5, 6-AN: n = 6 biological replicates. Scale bars are 10μm. G6P – glucose 6-phosphate, F6P – fructose 6-phosphate, F16BP – fructose 1,6-bisphosphate.

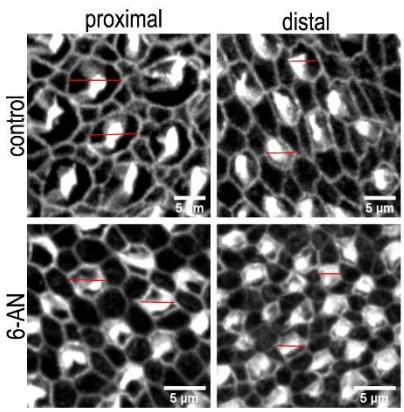

Figure 7 Supplement 1. Differences in the HC luminal surface area and gross bundle morphology in proximal and distal BP regions from explants treated with control or 6-AN containing medium.
Images are Maximum z-projections of Phalloidin stained BP explants from the proximal and distal BP regions. Explants were maintained from E6.5 for 7 days *in vitro* (equivalent to E13.5) in either control medium or that supplemented with the ppp inhibitor 6-AN. Phalloidin staining depicts differences in hair cell luminal surface area and gross bundle morphology between proximal and distal regions. Red lines indicate the size difference in HC luminal surface area between control and 6-AN-treared cultures. Scale bars are 5 μm.

However, contrary to all other inhibitor treatments, YZ9 was unique because it did not produce a significant interaction term in our 2-way ANOVA (Figure 6 Supplement 1C, supplementary table 1). Because the interaction term indicates the detection of differences in the proximal-distal gradient that are induced by YZ9 treatment relative to the control group, the result demonstrates that YZ9 is significantly less disruptive to the proximal-distal gradient than 2-DOG, SAM and 6-AN treatments. (Figure 7 supplement 1, supplementary table 1). These findings suggest that tonotopic patterning and specification of HC positional identity are regulated by glucose flux in the main branch of glycolysis upstream of PFK.

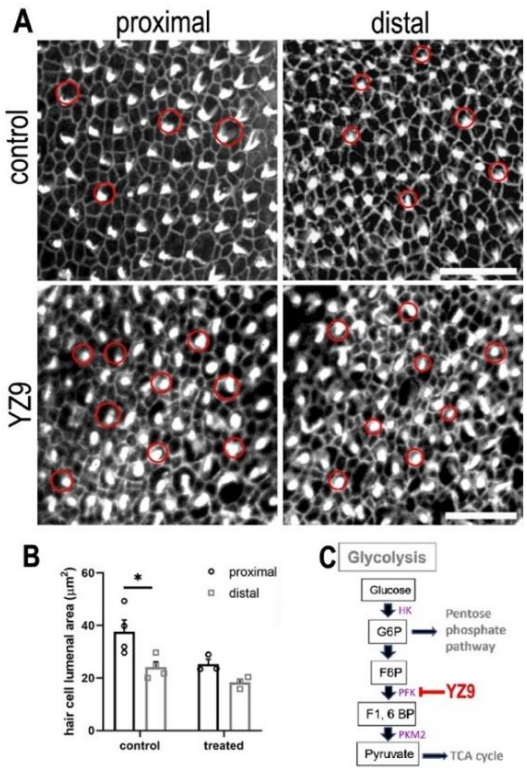

Figure 7 Supplement 2. Inhibiting phosphofructokinase has no effect on hair cell positional identity in the developing BP.
(A) Maximal z-projections showing Phalloidin staining in proximal and distal BP regions of control and YZ9-treated explants.
(B) Blocking glycolysis at the level of PFK between E6.5 and E13.5 had no effect on hair cell morphology along the tonotopic axis. Hair cell circumference was quantified in 2500 μm^2 areas in proximal (blue bars) and distal (orange bars) regions, showing no difference in size or density after treatment with 1μM YZ9.
(C) Schematic illustrating the inhibitory action of YZ9 in the glycolytic pathway.
Data are mean ± SEM. * $p < 0.05$ 2-way ANOVA. Controls: n = 4, YZ9: n = 3. Scale bars are 20 μm. Red circles indicate size hair cell luminal surface area between control and YZ9-treated explants. G6P – glucose 6-phosphate, F6P – fructose 6-phosphate, F1, 6BP – fructose 1,6-bisphosphate.

Pyruvate mediated OXPHOS in mitochondria maintains the overall progression of HC development. In the developing BP, live imaging of mitochondrial activity revealed no difference in OXPHOS along the tonotopic axis. To determine whether mitochondrial metabolism influences tonotopic patterning during BP development, we blocked uptake of glycolytically-derived pyruvate into mitochondria by inhibiting the mitochondrial pyruvate carrier (MPC) with UK5099 (Figure 8B). [41] Preventing pyruvate uptake into mitochondria decreases TCA cycle activity, as a result, impairs OXPHOS and ATP production in the electron transport chain (Figure 8B). HCs in explants treated with UK5099 between E6.5 and E13.5 did not develop with normal HC morphologies at all positions along the BP. HCs also displayed immature stereociliary bundles or lacked them completely in both proximal and distal regions (Figure 8A, C, red arrows). To determine whether this effect was due to an overall arrest in HC development, explants were established at E8.5, by which time positional identity is specified but bundles are not yet developed and maintained for 7 days *in vitro* to the equivalent of E15.5.

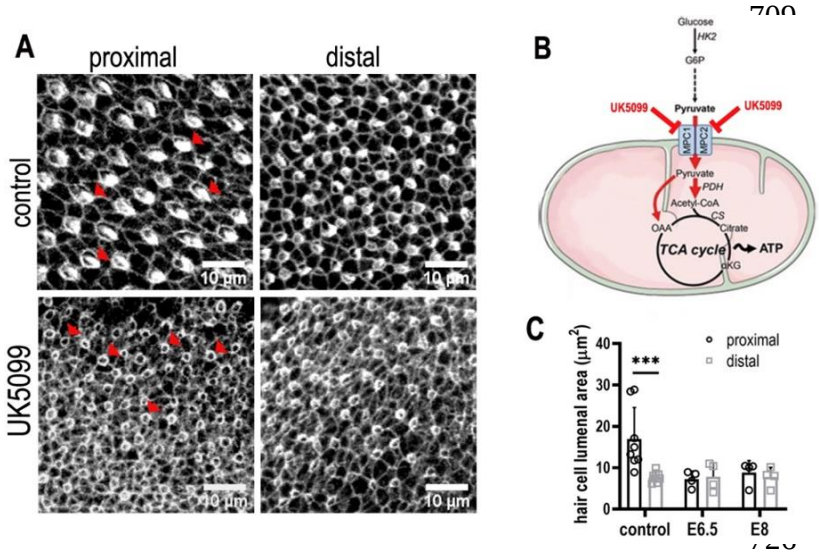

Figure 8. Mitochondrial OXPHOS is necessary for the normal developmental progression of hair cells but not positional identity.
(A) Hair cell morphology at the surface of the BP epithelium in explants stained with Phalloidin. Cultures were established at E6.5 and maintained for 7 days *in vitro* in control medium of that supplemented with the mitochondrial inhibitor UK5099.
(B) Blocking pyruvate uptake into mitochondria with UK5099 disrupts normal TCA cycle activity and thus mitochondrial OXPHOS by blocking uptake of pyruvate through the mitochondrial pyruvate carrier (MPC1/MPC2).
(C) Blocking mitochondrial metabolism Between E6.5 and E13 resulted in developmental abnormalities in HCs along the BP and a significant reduction in hair cell size in the proximal region. Stereocilia bundles of hair cells in the proximal BP region (red arrows) appeared immature compared to controls and those at the distal end. To determine whether mitochondrial OXPHOS acts during a specific developmental time window, cultures were treated with 1µM UK5099 for 7 days *in vitro* from E6.5 or for 7 days *in vitro* from E8.5. These times points are both be equivalent developmentally to E13.5. for Proximal hair cells showed no recovery following UK5099 wash-out. Data are mean ± SEM. * $p < 0.05$, 2-way ANOVA.

Compared to control explants, those treated with UK5099 displayed no tonotopic patterning at any position along the BP and showed immature gross bundle morphology along the entire organ (Figure 8A, C). The role that mitochondria play in shaping HC morphologies and functional properties at different frequency positions is at present unclear and requires further investigation. Our data suggest that mitochondrial metabolism plays a more significant role in maintaining the overall progression of HC development rather than regulating patterning along the frequency axis.

Treatment	2-way RM ANOVA p-values		significant interaction?
	overall proximal-distal differences	interaction	
6AN	0.0005	0.0002	***
2-DOG	0.0002	0.0001	***
SAM	0.0011	0.0003	***
YZ9	0.0055	0.1962	ns
BMP7	0.0001	0.0001	***
UK-5099	0.0287	0.0112	*

Supplementary Table 1. 2-way repeated measures ANOVA results for all *in vitro* culture experiments. p-values in the left-hand column indicate whether proximal-distal differences in HC luminal SA were detected in control or inhibitor treatment groups. The p-values in the *interaction* column indicate whether the proximal-distal differences in HC luminal SA changed after inhibitor treatment. YZ9, the inhibitor of PFK was the only treatment which did not produce a significant interaction, indicating a reduced capacity to abolish flatten tonotopic morphology compared to other treatments.

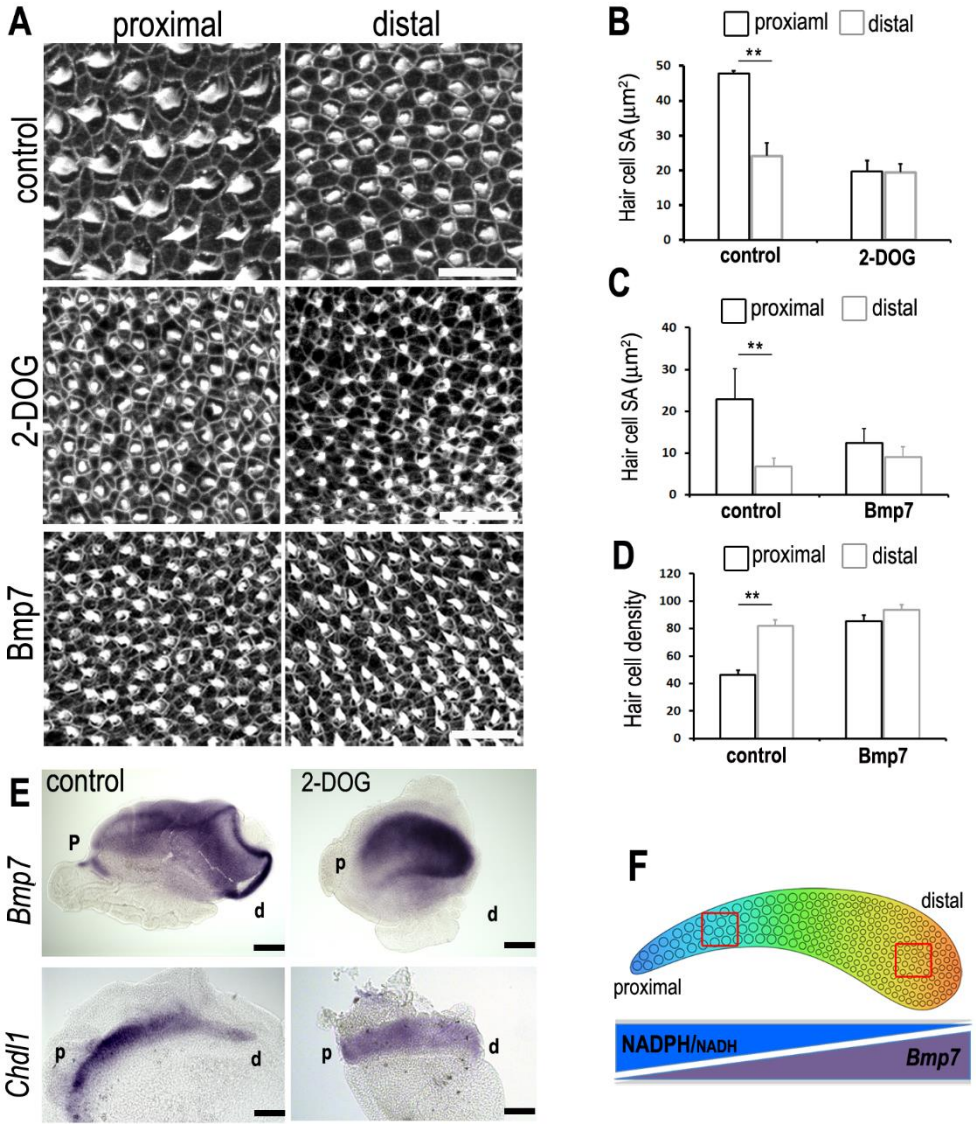

Figure 9. A tonotopic gradient in NAD(P)H producing glucose metabolism specifies hair cell positional identity along the BP by regulating gradients of Bmp7 and Chordin like-1.

(A) Phalloidin staining at the surface of BP explants in the proximal and distal regions. Explants were established at E6.5 and incubated for 7 days *in vitro* in control medium or medium containing 2-DOG + NaP or Bmp7.

(B-C) Treatment with 2-DOG or Bmp7 induced hair cell morphologies consistent with a more distal phenotype in the proximal BP. Hair cell luminal surface area was determined using Phalloidin staining at the cuticular plate in 2500 μm^2 areas.

(D) Treatment with Bmp7 between E6.5 and E13.5 equivalent results in increased hair cell density in the proximal BP region. Hair cell density was counted in proximal and distal BP regions using defines ROIs of 100,000 μm^2.

(E) Treatment of explant cultures with 2-DOG + NaP from E6.5 for 7 days *in vitro* disrupts the normal tonotopic expression of Bmp7 and its antagonist Chordin like-1. Images show *in situ hybridisation* for *Bmp7* and *Chordin like-1* in BP whole-mounts treated with 2-DOG +NaP from E6.5 for 7 days *in vitro*.

(F) Schematic of the chick BP, showing the graded differences in hair cell size and density along the tonotopic axis. The opposing gradients in Bmp7 activity and in cellular NAD(P)H/NADH (glycolysis) are indicated. Red boxes indicate regions of measurement for HC luminal SA and cell density.

(2-DOG) Controls: n=6, 2-DOG: n=6 Data mean ± SEM. * $p < 0.05$ 2-way ANOVA. (Bmp7) Controls: n=11. Bmp7 n=10. Data mean ± SEM. * $p < 0.05$ 2-way ANOVA. Scale bars (A) control scale bar is 20 µm, DOG and Bmp7 are 50 µm. Scale bars for *in situ* data (E) are 10µm.

Glucose metabolism regulates expression of Bmp7 and Chdl-1 along the tonotopic axis

In many developing systems, gradients of one or more morphogen act to regulate cell fate, growth and patterning along a given axis [42,43]. In the chick cochlea, reciprocal gradients of Bmp7 and its antagonist Chdl-1 play key roles in determining positional identity. As disruption of both the normal gradient in Bmp7 activity [17] and glycolysis induce similar patterning phenotypes (Figure 6, Figure 9A-D), we sought to identify a potential crosstalk between metabolism and the *Bmp7-Chdl-1* signalling axis.

To investigate the regulatory effects of glucose metabolism on the expression gradients of Bmp7 and Chdl-1, explants were established at E6.5 and maintained for 72 hours *in vitro* (equivalent of E9.5) in control medium or that containing 2-DOG + sodium pyruvate. Whole-mount *in situ* on explant cultures showed that disrupting glycolysis altered the normal expression gradients in both Bmp7 and Chdl-1 along the BP (Figure 9E). Specifically, following treatment with 2-DOG, Bmp7 expression appeared to increase into the proximal BP region and the expression of Chdl-1 decreased along the entire length of the organ. Normalised Bmp7 expression along the BP following treatment with 2-DOG could explain the expansion of distal-like HC morphologies into the proximal region. Taken together, our findings indicate a causal link between glycolysis and Bmp7 signalling in specifying HC positional identity during development. However, to determine whether cells in the proximal BP have truly acquired a distal-like fate, a detailed physiological analysis is required. In future studies, it will be important to understand how altering metabolism along the epithelium affects morphological development and functional properties of the stereociliary bundle and the intrinsic electrophysiological properties of the HCs at different frequency positions.

Discussion

To successfully address hearing and balance deficits following damage, aging or ototoxic insult, we must be able to generate new, functionally correct HCs from within the sensory epithelium at the correct positions along the frequency axis. As high frequency HCs are more vulnerable to insult than low frequency HCs, it is essential we understand the specific factors and signalling pathways that specify these HC subtypes along the tonotopic axis.

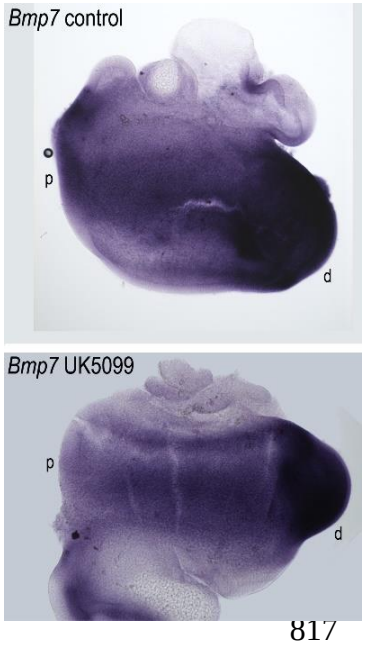

Figure 9 supplement 1. Treatment of explant cultures with UK5099 from E6.5 for 7 days *in vitro* does not elicit marked changes in the normal expression of Bmp7along the BP. Images show *in situ hybridisation* for *Bmp7* in BP whole-mounts treated with UK5099 from E6.5 for 7 days *in vitro*.

Generating new HCs that recapitulate the features of those in a healthy cochlea requires a detailed knowledge of the cell biology that drives their formation. Further to this, it is important we resolve how both HCs and SCs navigate the path of maturation and survival within their surrounding niche along the cochlea. Previous studies have focused largely on understanding the role of transcription factors in HC formation and how manipulation of these pathways in the adult inner ear can be exploited to promote regeneration [34,44-47]. Taking a novel approach, we here, characterised regional differences in metabolism along the developing BP and explored a role for coordinated signalling between known developmental pathways and metabolism in the establishment of HC positional identity.

NAD(P)H FLIM reveals a gradient in metabolism along the tonotopic axis of the developing chick cochlea.

Using NAD(P)H FLIM, we uncovered a proximal-to-distal gradient in cellular NADPH resulting from tonotopic differences in PPP-linked metabolism. The cellular basis for this gradient were further investigated by exploring potential differences in mitochondrial activity and glucose uptake along the developing BP, both of which contribute to the generation of cellular NADPH. Given the uniform gradients in both TMRM fluorescence and IDH3A expression we concluded that the NADPH gradient reported by τ_{bound} results primarily from tonotopic differences in cytosolic but not mitochondrial glucose metabolism. Without a reliable method to trace the fate of glucose following its uptake by GLUT transporters and subsequent phosphorylation by HK in glycolysis, it is challenging to resolve the discrepancy between 2-NBDG fluorescence and the NADPH gradient. Uniform glucose uptake and mitochondrial activity along the tonotopic axis coupled with the gradient in NADPH/NADH indicates an increased glucose flux through the PPP relative to the main glycolytic pathway.

PPP metabolism HC size and differentiation

The PPP functions in parallel to glycolysis in most living cells. It comprises an oxidative part regulated by the NADPH- generating enzyme glucose-6-phosphate dehydrogenase (G6PDH) and a non-oxidative part involving the reversible transketolase and transaldolase reactions, which interchange metabolites with glycolysis. The oxidative branch plays an important role in antioxidant defences and the non-

oxidative branch provides the necessary precursors for synthesis of nucleic and fatty acids. PPP-derived NADPH is utilised in proliferating cells during development where it regulates cell cycle progression, differentiation, and cell size [48,49]. In plants, cell size is determined by the opposing processes of growth and division [50], and PPP activity regulates the signalling pathways that coordinate these [51]. Mechanisms linking cell growth, cell cycle progression and metabolism are poorly understood in the context of development within complex tissues such as the cochlea. In the BP, HCs exit the cell cycle in three progressive waves following a centre-to-periphery progression beginning at E5. During this process, both HCs and SCs are added in apposition, to the edges of the band of post-mitotic cells that preceded them [21]. HC differentiation then begins in the distal portion of the BP at around E6 and extends proximally along the cochlea expanding across the width of the tissue [16,52,53]. As increased cell size is linked with increased G6PDH activity [49] the higher glucose flux in the proximal BP region may be a consequence or regulator of the graded differences in HC size. Differential PPP metabolism, reported here by a gradient in NADPH FLIM, may therefore play a role in setting up tonotopic differences in HC size along the organ, an essential feature for auditory coding [54].

A role for the PPP in HC electrical resonance and temporal coding

Cell size, cell membrane composition and metabolic rate are tightly correlated [55]. PPP metabolism is closely linked with de novo synthesis of lipids and cholesterol [56], which form an integral part of the cell membrane. Functional interactions between ion channel complexes in the membrane and the local lipid environment have been described previously in mammalian [57,58] and avian HCs [59]. Frequency tuning in the BP relies on the intrinsic electrical properties of the HCs themselves, where graded differences in the number and kinetics of voltage-gated calcium channels (VGCCs) and calcium-sensitive (BK type) potassium channels underlie the ability of HCs to resonate electrically in response to sound [54]. Studies in HCs from the mature BP showed that depleting membrane cholesterol causes a significant reduction in BK channel conductance, displaces channels from nearby VGCCs and induced a marked increase in total VGCC number. Membrane lipid composition has not been characterised along the tonotopic axis during development. However, given that HCs in the proximal BP region typically have a larger BK channel conductance and are more sensitive to perturbations in calcium, one can presume that cholesterol depletion in this region would have the greatest consequences for HC physiology and auditory coding. These findings may implicate a role for graded PPP activity in regulating HC electrical resonance.

Changes in the cell-specific expression of metabolic enzymes during development reflect divergence of HC and SC metabolic states

The enzymes LDHA and IDH3 are key regulators of metabolic reprogramming between glycolysis and OXPHOS. Lactate dehydrogenase (LDH) catalyses the interconversion of pyruvate and lactate using NAD^+ as a cofactor. LDHA catalyses the conversion of pyruvate to lactate producing NAD^+ and LDHB, the conversion of lactate to pyruvate and producing NADH (Figure 5). LDHA is highly expressed in conditions of low oxygen such as those in the cochlea [60] or during periods of reduced ETC activity observed commonly in the immature mitochondria of developing cells [61]. LDHB maintains high levels of pyruvate and is expressed abundantly in tissues with a dependence on OXPHOS [62]. We observed marked changes in the cell-specific expression of LDHA and LDHB throughout development (Figure 5) consistent with a metabolic divergence between HCs and their auxiliary SCs. The coincident downregulation of LDHA and upregulation of LDHB reflects increased OXPHOS and coincides with an increase in mitochondrial activity and IDH3A expression. Together, these findings are consistent with HCs in the adult cochlea relying predominantly on mitochondrial OXPHOS [63] and LDHB-derived pyruvate [64]. The loss of LDHA expression and restriction of LDHB to HCs between E9 and E14 reflects their increased dependence on mitochondrial OXPHOS during functional maturation. The mechanisms linking metabolic reprogramming with the transcriptional mechanisms driving HC and SC fates is still unclear. Studies in various cancer cells have however shown that LDHA expression regulates SOX2, which although required for specification of both cell fates, becomes restricted to SCs as development proceeds [34,65].

A causal link between metabolism and morphogen signalling during development sets up HC positional identity.

Morphogen signalling gradients have well defined roles in directing cell identity along developing axes, where distinct cell subtypes are determined as a function of morphogen concentration at different positions along them [42,66,67]. We showed previously that reciprocal gradients in Bmp7 and Chd-l1 set up positional identity in HCs along the developing BP [17]. The gradient of Bmp7 is regulated by Shh emanating from the distal BP region [68]. We here identify a proximal-to-distal gradient in glucose metabolism that regulates the morphological properties associated with HCs at different positions along the tonotopic axis. Disrupting this gradient using 2-DOG, SAM or 6-AN mimics the effects of altered Shh, Bmp, or Chd-l1 signalling [17,68], inducing distal-like HC phenotypes in the proximal BP region. Our findings therefore indicate a causal link between developmental and metabolic pathways along the tonotopic axis during HC formation.

In the presomitic mesoderm, metabolism regulates morphogen signalling such that opposing gradients in glycolytic and oxidative pathways drive elongation of the body axis. Here, glycolysis acts to generate a gradient in intracellular pH (pHi) along the axis, which, in turn establishes graded activity of FGF and Wnt signalling pathways [11-13]. The pHi gradient along the developing body axis acts to specify neuronal and mesodermal cell fates by modulating the acetylation and thus stability of beta catenin [11]. Given the importance of Wnt signalling in cochlear development and HC formation, it would be important to determine whether the gradient in glucose metabolism along the developing BP establishes similar differences in pHi and beta catenin acetylation. Impaired glycolysis has been shown to regulate Hedgehog (Hh) signalling in the developing wing disc by interacting with smoothened at the primary cilia [69]. One could therefore hypothesise that the distalisation of HCs in the proximal region after 2-DOG treatment occurs due to increased Shh activity enhancing the range of Bmp7 signalling.

Given the crosstalk between Wnt and Shh signalling in regulating proliferation in sensory progenitors [70], understanding their interrelationship with metabolism during this process has significant impact for HC regeneration. Untangling the interactions between components of the Shh, Bmp7 and glycolytic signalling networks will further our understanding of how hair cells might be morphologically specified for auditory coding during their formation. Additionally, from what we understand about frequency selectivity in vertebrates [71], recapitulation of tonotopy will require that these gradients, and their associated signalling networks, scale correctly in different inner ear sensory patches and across species with varying head size and cochlear lengths. Understanding how the mechanical constraints associated with different sense organs modulates these networks at the cellular level will be important for the advancement of inner ear organoid models.

Materials and Methods

Embryo care and procedures

Fertilized White Leghorn chicken (*gallus gallus domesticus*) eggs (Henry Stewart & Co. LTD, UK)) were incubated at 37.5°C in an automatic rocking incubator (Brinsea®) until use at specific developmental stages between E6 and E16. Embryos were removed from their eggs, staged according to Hamburger and Hamilton (1951) and subsequently decapitated. All embryos were terminated prior to hatching at E21. All procedures were performed in accord with United Kingdom legislation outlined in the Animals (Scientific Procedures) Act 1986.

Preparation of BP explants for live imaging studies

BPs were collected chick embryos between E7 and E16, and explants were established at E13 to E16 in accord with United Kingdom legislation outlined in the Animals (Scientific Procedures) Act 1986. Explants were placed onto Millicell cell culture inserts (Millipore ®) and incubated overnight at 37°C. maintained in medium 199 Earl's salts (M199) (GIBCO, Invitrogen) containing 2% fetal bovine serum and 5 mM HEPES buffer (Life Technologies). For live imaging experiments cultures were transferred to glass-bottom 50 mm MatTek dishes and held in place using custom-made tissue harps (Scientifica). Cultures were maintained in L-15 medium at room temperature throughout the experiment.

Basilar papilla culture

Basilar papillae (BPs) were isolated from embryos incubated for between 6 (E6.0) and 8 E8.0) days and maintained in chilled Leibovitz's L-15 media (GIBCO, Invitrogen). Papillae were dissected as described previously [72] and cultured nerve-side-down on Millicell cell culture inserts (Millipore ®). Cell culture inserts were placed into 35 mm culture dishes containing 1.5 mL of medium 199 Earl's salts (M199) (GIBCO, Invitrogen) supplemented with 5 mM HEPES buffer and 2% fetal bovine serum (FBS). Papillae were maintained in M199 medium plus vehicle (control media) for up to 7 DIV until the equivalent of embryonic day 13.5 (E13.5). For all treatments, a minimum of four samples were analysed. The following factors were applied to experimental BPs in culture at the specified concentrations: 2-Deoxyglucose (2-DOG) 2mM (SIGMA), Sodium Pyruvate (NaP) 5mM (SIGMA), 6-Aminonicotinamide (6AN) 2μM (SIGMA), *S*-(5'-Adenosyl)-*L*-methionine chloride dihydrochloride (SAM) 50μM (SIGMA), YZ9 1μM (SIGMA). For 2-DOG wash-out experiments, cultures were treated for 24 or 48 hours followed by wash out with control medium for the remainder of the experiment up to 7 days. For paired controls, medium was also changed at 24 and 48 hours in culture. At the conclusion of each experiment (7 days *in vitro*), cultures were fixed in 4% paraformaldehyde (PFA) for 20 minutes at room temperature, washed thoroughly three times with 0.1 M phosphate buffered saline (Invitrogen) and processed for immunohistochemistry.

Fluorescence lifetime imaging

NAD(P)H FLIM was performed on an upright LSM 510 microscope (Carl Zeiss) with a 1.0 NA 40x water-dipping objective using a 650-nm short-pass dichroic and 460±25 nm emission filter. Two-photon excitation was provided by a Chameleon (Coherent) Ti:sapphire laser tuned to 720 nm, with on-sample powers kept below 10 mW. Photon emission events were registered by an external detector (HPM-100, Becker & Hickl) attached to a commercial time-correlated single photon counting electronics module (SPC-830, Becker & Hickl) contained on a PCI board in a desktop computer. Scanning was

performed continuously for 2 min with a pixel dwell time of 1.6µs. Cell type (HC vs SC) and z-position within the epithelium was determined prior to FLIM analysis using the mitochondrially targeted fluorescent dye tetramethylrhodamine methyl ester (TMRM). The dye was added to the recording medium, at a final concentration of 350 nM, 45 min before imaging. TMRM fluorescence was collected using a 610±30 nm emission filter. Excitation was provided at the same wavelength as NAD(P)H to avoid possible chromatic aberration. The 585±15 nm emission spectrum of TMRM ensured its fluorescence did not interfere with acquisition of the NAD(P)H FLIM images.

FLIM data analysis

Following 5 x 5 binning of photon counts at each pixel, fluorescence decay curves of the form [14],

$$I(t) = Z + I_0\left([1 - \alpha_{\text{bound}}]e^{-t/\tau_{\text{free}}} + \alpha_{\text{bound}}e^{-t/\tau_{\text{bound}}}\right)$$

were fit to the FLIM images using iterative reconvolution in SPCImage (Becker & Hickl), where Z allows for time-uncorrelated background noise. Matrices of the fit parameters τ_{free}, α_{bound} and τ_{bound} and the total photons counted were at each pixel, were exported and analysed for hair cells and supporting cells, and proximal and distal BP regions, using SPCImage and ImageJ software packages.

2-NBDG and TMRM live imaging

The auditory sensory epithelia were isolated from E7, E9, E14 and E16 chick embryos in chilled L-15 medium. BPs were subsequently incubated in 1mM solution of 2-NBDG (N13195, Thermo Fisher Scientific) in L-15 medium at room temperature for 1 hour. The medium was then replaced with a fresh solution of 1mM 2-NBDG and 350 nm TMRM (T668, Thermo Fisher Scientific) in L-15 and incubated for a further hour at room temperature. Afterwards, epithelia were washed several times with fresh medium containing 350 nM TMRM and were mounted in a 3.5 mm glass bottom MatTek dish. 3D image stacks with an optical thickness of 1µm were captured using a Leica SP5 confocal microscope with an HCX PL APO 63×/1.3 GLYC CORR CS (21 °C) objective.

Immunohistochemistry

Inner ear tissue was collected at various developmental stages, fixed for 20 min to one hour in in 0.1 M phosphate buffered saline (PBS) containing 4% paraformaldehyde (PFA), and processed for whole-mounts immunohistochemistry. The auditory sensory epithelium was then fine dissected and permeabilized in PBS containing 0.3% Triton for 30 min before immunostaining using standard procedures. Samples were stained with primary antibodies for LDHA 1:75 (Genetex GTX101416) and IDH3A 1:75 (ab228596, Abcam) and Calbindin 1:50 (ab82812, Abcam). Antibody staining was

visualized using secondary antibodies conjugated to either Alexa 488 or Alexa 546 (Invitrogen). Cultures were incubated with all secondary antibodies for 1 hour at room temperature 1:1000, washed thoroughly in 0.1 M PBS. Samples were then incubated for an additional hour with either Alexa Fluor-conjugated Phalloidin-546 (Invitrogen) to label filamentous actin and DAPI 1:1000 to label cell nuclei. Tissue samples were mounted using either Prolong Gold antifade reagent (Invitrogen). 3D image stacks of mounted samples were captured using a Leica SP5 confocal microscope with an HCX PL APO 63×/1.3 GLYC CORR CS (21 °C) objective.

EdU staining

Control or 2-DOG-treated cultures were incubated for 48 hours in 10 μM 5-ethynyl-2'-deoxyuridine (EdU) from embryonic day 8 (E8) to embryonic day 10 (E10). Cultures were subsequently fixed for 15 minutes in 4% PFA at room temperature and then washed in 0.1M PBS. Explants were then processed for EdU staining following the Click-iT® EdU 488 protocol (Thermo Fischer Scientific).

Image analysis

Analysis of z-stacks from IHC stains as well as 2-NBDG and TMRM live imaging experiments was carried out using the Fiji distribution of imageJ. For each sample, a z-plane 2 µm beneath the surface of the epithelium was chosen for further analysis. For each of these selected z-planes, a 100 µm x 100 µm region of interest (ROI) was chosen containing intact tissue in which all HCs were optimally orientated. Mean fluorescence intensity of the tissue was measured for ROIs at E7, E9 and E10 timepoints. At E14 and E16, HCs were manually segmented. HC labels were dilated by 3 µm, which provided selections which included both hair cells and their surrounding SCs. By subtracting the hair cell segmentation from the dilated label, we were thus able to measure the fluorescence intensity of whole HCs separately from their surrounding support cells in the 2-NBDG and LDHA data. A similar approach was adopted when measuring TMRM and IDH3A fluorescence intensity at E14 and E16. However, we noticed that signal was concentrated around the HC periphery. In order to ensure that the fluorescence intensity best reflected only the mitochondria and was not reduced by the low fluorescence from the centre of each HC, we measured mean fluorescence intensity only up to 2 µm from the cell membrane. Likewise, for TMRM and IDH3A data at E7 and E9, mitochondria were segmented using Fiji's auto-local thresholding (Niblack) prior to intensity measurements, to avoid a biased estimate of fluorescence intensity due to empty space surrounding each mitochondrion.

Analysis of hair cell morphology

Data were analysed offline using image J software. Hair cell luminal surface area and cell size were used as indices for HC morphology along the tonotopic axis. To determine the hair cell density, the luminal surfaces of hair cells and cell size, cultures were labelled with phalloidin and DAPI. Then, the number of hair cells in 50 µm × 50 µm regions of interest (2,500 μm^2 total area) located in the proximal and distal BP regions were determined. Proximal and distal regions were determined based a calculation of the entire length of the BP or explant. In addition, counting ROIs were placed in the mid-region of the BP along the neural to abneural axis to avoid any confounding measurements due to radial differences between tall and short hair cells. For each sample, hair cells were counted in four separate ROIs for each position along the BP. Luminal surface areas were determined by measuring the circumference of individual hair cells at the level of the cuticular plate.

Statistical testing and analyses.

All data were assessed for normality prior to application of statistical tests, with a threshold of $p<0.05$ used for determining significance. When comparing between proximal and distal regions within the same tissue explant, paired t-tests with unequal variance were used. This statistical approach was chosen given that measurements were made from different regions within the same sample and were therefore not independent from each other. Comparisons made between different developmental stages were assumed independent from one another and thus here, independent t-tests and 2-way ANOVAs were used.

In situ hybridisation

Inner ear tissue was dissected and fixed in 4% PFA overnight at 4 °C. Tissue was subsequently washed three times for 30 min in 0.1 M PBS and subsequently dehydrated in methanol (25–100%). Tissue was stored at −20 °C until use. Immediately before the *in situ* protocol, tissue was rehydrated using a reverse methanol gradient (100–25%). Complimentary digoxigenin-labelled RNA probes for *Bmp7* were kindly provided by Doris Wu (NIDCD, NIH). *Chd-l1* was synthesised as described previously [17]. All *in situ* hybridization reactions were performed as described previously.

RNAscope

Gene-specific probes and the RNAscope® Fluorescent Multiplex Reagent Kit (320850) were ordered form Advanced Cell Diagnostics. Basilar papillae were collected from E8-E10 chick embryos, fixed overnight in 4% paraformaldehyde, and subsequently cryopreserved through a sucrose gradient (5%, 10%, 15%, 20%, and 30%). Samples were embedded in cryomolds using Tissue-Tek O.C.T compound

and sectioned on a cryostat at 10-12 μm thickness. RNAscope hybridization protocol was carried out based on the manufacturer's (ACD) suggestions. All fluorescent images were obtained on a Zeiss LSM 900 confocal microscope.

RNA-seq analysis

For bulk RNA-seq analysis, all genes with a Log_2 >1 were considered significantly expressed in the distal BP region and all genes with a Log_2 <1 significantly expressed in the proximal BP region. Statistical significance levels were calculated by one-way ANOVA. For a gene to be considered 'differential', at least one region of the BP (proximal, middle or distal) was required to be ≥ 0.5 RPKM. A fold change of ≥ 2 was imposed for the comparison between distal and proximal regions. A final requirement was that middle samples had to exhibit RPKM values mid-way between proximal and distal regions to selectively capture transcripts with a gradient between the two ends. Bulk Affymetrix data were analysed for differentially expressed mRNAs encoding metabolic effector proteins that regulate cellular NADPH levels. Microarray signals were normalized using the RMA algorithm. The mRNAs expressed at significantly different levels in distal versus proximal BP were selected based on ANOVA analysis using the Partek Genomics Suite software package (Partek, St. Charles, MO, USA). ***** = $p < 0.05$. For detailed description of analysis and protocols please refer to Mann at al., 2014.

Acknowledgements

The authors wish to thank Matthew Kelley, Dan Jagger, Jeremy Green, Michael Duchen, Gyorgy Szabadkai and Jonathan Gale and Val Yianni for providing important comments and critical discussion on earlier versions of the manuscript. This project was supported by funds from the King's Prize Fellowship (King's College London) (ZFM) and the Biotechnology and Biological Sciences Research Council (BBSRC) grant BB/V006371/1 (ZFM).

Author contributions

ZFM, TSB conceptualised the study and experimental design.

ZFM, TSB, JO, CS MA developed and executed the methodology.

ZFM, JO, CS analysed and interpreted the data.

ZFM, TSB, JO wrote and edited the manuscript, which was reviewed by all contributing authors. ZFM is the guarantor of this study, with responsibility for integrity and accuracy of the data.

References

1 Gordon-Salant, S. Hearing loss and aging: new research findings and clinical implications. *J Rehabil Res Dev* **42**, 9-24, doi:10.1682/jrrd.2005.01.0006 (2005).

2 Fettiplace, R. & Nam, J. H. Tonotopy in calcium homeostasis and vulnerability of cochlear hair cells. *Hear Res* **376**, 11-21, doi:10.1016/j.heares.2018.11.002 (2019).

3 Wu, F., Xiong, H. & Sha, S. Noise-induced loss of sensory hair cells is mediated by ROS/AMPKalpha pathway. *Redox Biol* **29**, 101406, doi:10.1016/j.redox.2019.101406 (2020).

4 Forge, A. & Richardson, G. Freeze fracture analysis of apical membranes in cochlear cultures: differences between basal and apical-coil outer hair cells and effects of neomycin. *J Neurocytol* **22**, 854-867, doi:10.1007/BF01186357 (1993).

5 Ito, K. & Ito, K. Metabolism and the Control of Cell Fate Decisions and Stem Cell Renewal. *Annu Rev Cell Dev Biol* **32**, 399-409, doi:10.1146/annurev-cellbio-111315-125134 (2016).

6 Kinnaird, A., Zhao, S., Wellen, K. E. & Michelakis, E. D. Metabolic control of epigenetics in cancer. *Nat Rev Cancer* **16**, 694-707, doi:10.1038/nrc.2016.82 (2016).

7 Campbell, S. L. & Wellen, K. E. Metabolic Signaling to the Nucleus in Cancer. *Mol Cell* **71**, 398-408, doi:10.1016/j.molcel.2018.07.015 (2018).

8 Bhattacharya, D., Azambuja, A. P. & Simoes-Costa, M. Metabolic Reprogramming Promotes Neural Crest Migration via Yap/Tead Signaling. *Dev Cell* **53**, 199-211 e196, doi:10.1016/j.devcel.2020.03.005 (2020).

9 Kantarci, H., Gou, Y. & Riley, B. B. The Warburg Effect and lactate signaling augment Fgf-MAPK to promote sensory-neural development in the otic vesicle. *Elife* **9**, doi:10.7554/eLife.56301 (2020).

10 Chi, F., Sharpley, M. S., Nagaraj, R., Roy, S. S. & Banerjee, U. Glycolysis-Independent Glucose Metabolism Distinguishes TE from ICM Fate during Mammalian Embryogenesis. *Dev Cell* **53**, 9-26 e24, doi:10.1016/j.devcel.2020.02.015 (2020).

11 Oginuma, M. *et al.* A Gradient of Glycolytic Activity Coordinates FGF and Wnt Signaling during Elongation of the Body Axis in Amniote Embryos. *Dev Cell* **40**, 342-353 e310, doi:10.1016/j.devcel.2017.02.001 (2017).

12 Oginuma, M. *et al.* Intracellular pH controls WNT downstream of glycolysis in amniote embryos. *Nature* **584**, 98-101, doi:10.1038/s41586-020-2428-0 (2020).

13 Bulusu, V. *et al.* Spatiotemporal Analysis of a Glycolytic Activity Gradient Linked to Mouse Embryo Mesoderm Development. *Dev Cell* **40**, 331-341 e334, doi:10.1016/j.devcel.2017.01.015 (2017).

14 Blacker, T. S. *et al.* Separating NADH and NADPH fluorescence in live cells and tissues using FLIM. *Nat Commun* **5**, 3936, doi:10.1038/ncomms4936 (2014).

15 Tilney, L. G., Tilney, M. S. & DeRosier, D. J. Actin filaments, stereocilia, and hair cells: how cells count and measure. *Annu Rev Cell Biol* **8**, 257-274, doi:10.1146/annurev.cb.08.110192.001353 (1992).

16 Goodyear, R. & Richardson, G. Pattern formation in the basilar papilla: evidence for cell rearrangement. *J Neurosci* **17**, 6289-6301 (1997).

17 Mann, Z. F. *et al.* A gradient of Bmp7 specifies the tonotopic axis in the developing inner ear. *Nat Commun* **5**, 3839, doi:10.1038/ncomms4839 (2014).

18 Skala, M. C. *et al.* In vivo multiphoton microscopy of NADH and FAD redox states, fluorescence lifetimes, and cellular morphology in precancerous epithelia. *Proc Natl Acad Sci U S A* **104**, 19494-19499, doi:10.1073/pnas.0708425104 (2007).

19 Yu, Q. & Heikal, A. A. Two-photon autofluorescence dynamics imaging reveals sensitivity of intracellular NADH concentration and conformation to cell physiology at the single-cell level. *J Photochem Photobiol B* **95**, 46-57, doi:10.1016/j.jphotobiol.2008.12.010 (2009).

20 Thiede, B. R. *et al.* Retinoic acid signalling regulates the development of tonotopically patterned hair cells in the chicken cochlea. *Nat Commun* **5**, 3840, doi:10.1038/ncomms4840 (2014).

21 Katayama, A. & Corwin, J. T. Cell production in the chicken cochlea. *J Comp Neurol* **281**, 129-135, doi:10.1002/cne.902810110 (1989).
22 Blacker, T., Marsh, RJ., Duchen, MR., & Bain, AJ. . Activated barrier crossing dynamics in the non-radiative decay of NADH and NADPH. . *Chem. Phys.* **422**, 184-194 (2013).
23 Gafni, A. & Brand, L. Fluorescence decay studies of reduced nicotinamide adenine dinucleotide in solution and bound to liver alcohol dehydrogenase. *Biochemistry* **15**, 3165-3171, doi:10.1021/bi00660a001 (1976).
24 Monzack, E. L., May, L. A., Roy, S., Gale, J. E. & Cunningham, L. L. Live imaging the phagocytic activity of inner ear supporting cells in response to hair cell death. *Cell Death Differ* **22**, 1995-2005, doi:10.1038/cdd.2015.48 (2015).
25 Ying, W. NAD+/NADH and NADP+/NADPH in cellular functions and cell death: regulation and biological consequences. *Antioxid Redox Signal* **10**, 179-206, doi:10.1089/ars.2007.1672 (2008).
26 Yamada, K., Saito, M., Matsuoka, H. & Inagaki, N. A real-time method of imaging glucose uptake in single, living mammalian cells. *Nat Protoc* **2**, 753-762, doi:10.1038/nprot.2007.76 (2007).
27 Sanchez, T., Zhang, M., Needleman, D. & Seli, E. Metabolic imaging via fluorescence lifetime imaging microscopy for egg and embryo assessment. *Fertil Steril* **111**, 212-218, doi:10.1016/j.fertnstert.2018.12.014 (2019).
28 Gale, J. E., Marcotti, W., Kennedy, H. J., Kros, C. J. & Richardson, G. P. FM1-43 dye behaves as a permeant blocker of the hair-cell mechanotransducer channel. *J Neurosci* **21**, 7013-7025 (2001).
29 Hitosugi, T. & Chen, J. Post-translational modifications and the Warburg effect. *Oncogene* **33**, 4279-4285, doi:10.1038/onc.2013.406 (2014).
30 Fritz, P. J. Rabbit muscle lactate dehydrogenase 5; a regulatory enzyme. *Science* **150**, 364-366, doi:10.1126/science.150.3694.364 (1965).
31 Liu, J. *et al.* Aberrant FGFR Tyrosine Kinase Signaling Enhances the Warburg Effect by Reprogramming LDH Isoform Expression and Activity in Prostate Cancer. *Cancer Res* **78**, 4459-4470, doi:10.1158/0008-5472.CAN-17-3226 (2018).
32 Zhang, D. *et al.* Metabolic reprogramming of cancer-associated fibroblasts by IDH3alpha downregulation. *Cell Rep* **10**, 1335-1348, doi:10.1016/j.celrep.2015.02.006 (2015).
33 Lane, M. & Gardner, D. K. Lactate regulates pyruvate uptake and metabolism in the preimplantation mouse embryo. *Biol Reprod* **62**, 16-22, doi:10.1095/biolreprod62.1.16 (2000).
34 Driver, E. C. & Kelley, M. W. Development of the cochlea. *Development* **147**, doi:10.1242/dev.162263 (2020).
35 May, J. L. *et al.* IDH3alpha regulates one-carbon metabolism in glioblastoma. *Sci Adv* **5**, eaat0456, doi:10.1126/sciadv.aat0456 (2019).
36 Nagaraj, R. *et al.* Nuclear Localization of Mitochondrial TCA Cycle Enzymes as a Critical Step in Mammalian Zygotic Genome Activation. *Cell* **168**, 210-223 e211, doi:10.1016/j.cell.2016.12.026 (2017).
37 Barban, S. & Schulze, H. O. The effects of 2-deoxyglucose on the growth and metabolism of cultured human cells. *J Biol Chem* **236**, 1887-1890 (1961).
38 Zhao, J. *et al.* Low-dose 2-deoxyglucose and metformin synergically inhibit proliferation of human polycystic kidney cells by modulating glucose metabolism. *Cell Death Discov* **5**, 76, doi:10.1038/s41420-019-0156-8 (2019).
39 Pascale, R. M., Peitta, G., Simile, M. M. & Feo, F. Alterations of Methionine Metabolism as Potential Targets for the Prevention and Therapy of Hepatocellular Carcinoma. *Medicina (Kaunas)* **55**, doi:10.3390/medicina55060296 (2019).
40 Arnold, P. K. *et al.* A non-canonical tricarboxylic acid cycle underlies cellular identity. *Nature* **603**, 477-481, doi:10.1038/s41586-022-04475-w (2022).

41 Zhong, Y. *et al.* Application of mitochondrial pyruvate carrier blocker UK5099 creates metabolic reprogram and greater stem-like properties in LnCap prostate cancer cells in vitro. *Oncotarget* **6**, 37758-37769, doi:10.18632/oncotarget.5386 (2015).
42 Towers, M., Wolpert, L. & Tickle, C. Gradients of signalling in the developing limb. *Curr Opin Cell Biol* **24**, 181-187, doi:10.1016/j.ceb.2011.11.005 (2012).
43 Averbukh, I., Ben-Zvi, D., Mishra, S. & Barkai, N. Scaling morphogen gradients during tissue growth by a cell division rule. *Development* **141**, 2150-2156, doi:10.1242/dev.107011 (2014).
44 Shu, Y. *et al.* Renewed proliferation in adult mouse cochlea and regeneration of hair cells. *Nat Commun* **10**, 5530, doi:10.1038/s41467-019-13157-7 (2019).
45 Taylor, R. R. *et al.* Regenerating hair cells in vestibular sensory epithelia from humans. *Elife* **7**, doi:10.7554/eLife.34817 (2018).
46 Shibata, S. B. *et al.* Gene therapy for hair cell regeneration: Review and new data. *Hear Res* **394**, 107981, doi:10.1016/j.heares.2020.107981 (2020).
47 Tao, L. *et al.* Enhancer decommissioning imposes an epigenetic barrier to sensory hair cell regeneration. *Dev Cell* **56**, 2471-2485 e2475, doi:10.1016/j.devcel.2021.07.003 (2021).
48 Vander Heiden, M. G., Cantley, L. C. & Thompson, C. B. Understanding the Warburg effect: the metabolic requirements of cell proliferation. *Science* **324**, 1029-1033, doi:10.1126/science.1160809 (2009).
49 Vizan, P. *et al.* Modulation of pentose phosphate pathway during cell cycle progression in human colon adenocarcinoma cell line HT29. *Int J Cancer* **124**, 2789-2796, doi:10.1002/ijc.24262 (2009).
50 A, R. J. *et al.* Cell-size dependent progression of the cell cycle creates homeostasis and flexibility of plant cell size. *Nat Commun* **8**, 15060, doi:10.1038/ncomms15060 (2017).
51 Kaplon, J., van Dam, L. & Peeper, D. Two-way communication between the metabolic and cell cycle machineries: the molecular basis. *Cell Cycle* **14**, 2022-2032, doi:10.1080/15384101.2015.1044172 (2015).
52 Cotanche, D. A. & Sulik, K. K. The development of stereociliary bundles in the cochlear duct of chick embryos. *Brain Res* **318**, 181-193, doi:10.1016/0165-3806(84)90024-5 (1984).
53 Bartolami, S., Goodyear, R. & Richardson, G. Appearance and distribution of the 275 kD hair-cell antigen during development of the avian inner ear. *J Comp Neurol* **314**, 777-788, doi:10.1002/cne.903140410 (1991).
54 Fettiplace, R. & Fuchs, P. A. Mechanisms of hair cell tuning. *Annu Rev Physiol* **61**, 809-834, doi:10.1146/annurev.physiol.61.1.809 (1999).
55 Hulbert, A. J. & Else, P. L. Membranes as possible pacemakers of metabolism. *J Theor Biol* **199**, 257-274, doi:10.1006/jtbi.1999.0955 (1999).
56 Sykes, J. E., Lopes-Cardozo, M. & Van Den Bergh, S. G. Relationship between the pentose-phosphate pathway and the de novo synthesis of fatty acids and cholesterol in oligodendrocyte-enriched glial cultures. *Neurochem Int* **8**, 77-82, doi:10.1016/0197-0186(86)90103-8 (1986).
57 Hirono, M., Denis, C. S., Richardson, G. P. & Gillespie, P. G. Hair cells require phosphatidylinositol 4,5-bisphosphate for mechanical transduction and adaptation. *Neuron* **44**, 309-320, doi:10.1016/j.neuron.2004.09.020 (2004).
58 Gianoli, F., Risler, T. & Kozlov, A. S. Lipid bilayer mediates ion-channel cooperativity in a model of hair-cell mechanotransduction. *Proc Natl Acad Sci U S A* **114**, E11010-E11019, doi:10.1073/pnas.1713135114 (2017).
59 Purcell, E. K., Liu, L., Thomas, P. V. & Duncan, R. K. Cholesterol influences voltage-gated calcium channels and BK-type potassium channels in auditory hair cells. *PLoS One* **6**, e26289, doi:10.1371/journal.pone.0026289 (2011).
60 Prazma, J., Rodgers, G. K. & Pillsbury, H. C. Cochlear blood flow. Effect of noise. *Arch Otolaryngol* **109**, 611-615, doi:10.1001/archotol.1983.00800230047011 (1983).

61 Arrazola, M. S. *et al.* Mitochondria in Developmental and Adult Neurogenesis. *Neurotox Res* **36**, 257-267, doi:10.1007/s12640-018-9942-y (2019).

62 Hong, S. M. *et al.* Lactic acidosis caused by repressed lactate dehydrogenase subunit B expression down-regulates mitochondrial oxidative phosphorylation via the pyruvate dehydrogenase (PDH)-PDH kinase axis. *J Biol Chem* **294**, 7810-7820, doi:10.1074/jbc.RA118.006095 (2019).

63 Holmgren, M. & Sheets, L. Using the Zebrafish Lateral Line to Understand the Roles of Mitochondria in Sensorineural Hearing Loss. *Front Cell Dev Biol* **8**, 628712, doi:10.3389/fcell.2020.628712 (2020).

64 Tian, C. *et al.* Suppressed expression of LDHB promotes age-related hearing loss via aerobic glycolysis. *Cell Death Dis* **11**, 375, doi:10.1038/s41419-020-2577-y (2020).

65 Jiang, F., Ma, S., Xue, Y., Hou, J. & Zhang, Y. LDH-A promotes malignant progression via activation of epithelial-to-mesenchymal transition and conferring stemness in muscle-invasive bladder cancer. *Biochem Biophys Res Commun* **469**, 985-992, doi:10.1016/j.bbrc.2015.12.078 (2016).

66 Dessaud, E., McMahon, A. P. & Briscoe, J. Pattern formation in the vertebrate neural tube: a sonic hedgehog morphogen-regulated transcriptional network. *Development* **135**, 2489-2503, doi:10.1242/dev.009324 (2008).

67 Sagner, A. & Briscoe, J. Establishing neuronal diversity in the spinal cord: a time and a place. *Development* **146**, doi:10.1242/dev.182154 (2019).

68 Son, E. J. *et al.* Conserved role of Sonic Hedgehog in tonotopic organization of the avian basilar papilla and mammalian cochlea. *Proc Natl Acad Sci U S A* **112**, 3746-3751, doi:10.1073/pnas.1417856112 (2015).

69 Spannl, S. *et al.* Glycolysis regulates Hedgehog signalling via the plasma membrane potential. *EMBO J* **40**, e107925, doi:10.15252/embj.2021107925 (2021).

70 Wu, J. *et al.* The crosstalk between the Notch, Wnt, and SHH signaling pathways in regulating the proliferation and regeneration of sensory progenitor cells in the mouse cochlea. *Cell Tissue Res* **386**, 281-296, doi:10.1007/s00441-021-03493-w (2021).

71 Gleich, O., Dooling, R. J. & Manley, G. A. Audiogram, body mass, and basilar papilla length: correlations in birds and predictions for extinct archosaurs. *Naturwissenschaften* **92**, 595-598, doi:10.1007/s00114-005-0050-5 (2005).

72 Jacques, B. E. *et al.* The role of Wnt/beta-catenin signaling in proliferation and regeneration of the developing basilar papilla and lateral line. *Dev Neurobiol* **74**, 438-456, doi:10.1002/dneu.22134 (2014).